Université de Montréal

Cellular basis of flower and leaf primordium initiation in *Arabidopsis thaliana*: How to make an organ in three dimensions?

par Emilie ECHEVIN

Département de sciences biologiques

Faculté des arts et des sciences

Mémoire présenté

en vue de l'obtention du grade de Maîtrise

en Sciences biologiques

Octobre 2020

Université de Montréal

Faculté des études supérieures et postdoctorales

Ce mémoire intitulé:

Cellular basis of flower and leaf primordium initiation in* Arabidopsis thaliana*: How to make an organ in three dimensions?

Présenté par :

Emilie ECHEVIN

A été évalué par un jury composé des personnes suivantes :

Anne-Lise ROUTIER, directrice de recherche

Daniel KIERZKOWSKI, co-directeur de recherche

David MORSE, président-rapporteur

Anja GEITMANN, membre du jury

Résumé

Le développement d'un organisme multicellulaire requière la coordination de la croissance, détermination tissulaire et différenciation cellulaire. Cependant, alors que les bases de la génétique de la morphogenèse ont été rigoureusement étudiées, le processus permettant la conversion de l'activité génétique en des structures biologiques complexes est bien moins compris. Chez *Arabidopsis thaliana*, les feuilles et fleurs initiés à partir du Méristème Apical Primaire (MAP) ont une expression génétique casi similaire. Toutefois, leur forme est considérablement différente dès les premières étapes de leur développement. Une compréhension de ce paradoxe requière avant tout de précisément quantifier la croissance dans toutes les dimensions de ces organes. Dans cet article, je présente une méthode de quantification spatio-temporelle complète de la croissance et de la prolifération des feuilles et des fleurs chez *A. thaliana*. En analysant des séries d'images confocales, j'en ai conclu que la différence morphologique observée entre feuilles et fleurs émerge principalement d'une asymétrie de la distribution de la croissance entre leurs côtés abaxial et adaxial, tôt dans leur développement. Je montre que le tissue contribuant principalement au développement des primordia est la couche 2 (L2) chez les feuilles et la couche 3 (L3) chez les fleurs. Mes résultats préliminaires démontrent que les premiers signes de l'initiation d'organes est un changement de distribution de la croissance, et non de la prolifération. Dans le futur, en appliquant, par exemple, cette méthodologie à l'étude de gènes de développement, il sera possible de finalement réconcilier la morphogenèse et la génétique de l'initiation des plantes.

Mots-clés

Phyllotaxie, expansion cellulaire, division cellulaire, morphogenèse végétale, organogenèse, initiation d'organes, organes latéraux de l'apex, analyse d'images, MorphoGraphX

Summary

The development of a multicellular organism requires the proper coordination of growth, pattern determination and cell differentiation. Still, while the genetic basis of morphogenesis has been extensively studied, the process converting gene activity into intricate biological shapes is less understood. In *Arabidopsis thaliana*, flowers and leaves, both initiated from the shoot apical meristem (SAM), have a very similar genetic expression profile. Yet, their shape differs considerably from early developmental stages. A full comprehension of this paradox requires an accurate quantification of cellular growth in those organs. In this paper, I am presenting a methodology for the complete spatio-temporal quantitative analysis of growth and proliferation of initiating leaves and flowers in wild type *Arabidopsis thaliana*. By analyzing time series of leaf and flower confocal images, I conclude that the morphological differences observed between flowers and leaves mainly arises from asymmetrical distributions of growth between their adaxial and abaxial sides during their initiation. I show that the tissue that mainly contributes to the development of early primordium is the layer 2 (L2) in leaves, and the layer 3 (L3) in flowers. My preliminary results also demonstrate that the first signs of organ initiation are a change in growth distribution, not cell proliferation. In the future, by applying this methodology, for example, to study morphogen reporter lines, it could finally bridge the gap between the morphogenesis and the genetics of plant initiation.

Keywords

Phyllotaxis, cell expansion, cell division, morphogenesis, organogenesis, organ initiation, shoot lateral organs, image analysis, MorphoGraphX

Table des matières

Liste des illustrations

Liste des tableaux

Abbreviation list

CZ: Central Zone.

ITK: Insight Segmentation and Registration Toolkit ('ITK') developed previously (Barbier de Reuille, 2015).

L1, L2, L3…: Layer 1, Layer 2, Layer 3 (from outmost to inner most layer of the shoot apical meristem).

PZ: Peripheral Zone.

SAM: Shoot Apical Meristem.

Review article abstract

During the first year of my master, I contributed to the writing of a paper: “Growth and biomechanics of shoot organs” (*Journal of Experimental Botany* 70, 3573–3585, 2019 doi:10.1093/jxb/erz205). The full version of this paper is attached in the annex. The abstract is presented below:

Abstract

Plant organs arise through complex interactions between biological and physical factors that control morphogenesis. While there has been tremendous progress in the understanding of the genetics behind development, we know much less about how mechanical forces control growth in plants. In recent years, new multidisciplinary research combining genetics, live-imaging, physics, and computational modeling has begun to fill this gap by revealing the crucial role of biomechanics in the establishment of plant organs. In this review, we provide an overview of our current understanding of growth during initiation, patterning, and expansion of shoot lateral organs. We discuss how growth is controlled by physical forces, and how mechanical stresses generated during growth can control morphogenesis at the level of both cells and tissues. Understanding the mechanical basis of growth and morphogenesis in plants is in its early days, and many puzzling facts are yet to be deciphered.

Introduction

Quantitative analysis of confocal images is a powerful tool to understand development at cellular resolution. In plants, a vast diversity of organ morphology leads to the question of how plant organs acquire their shapes and sizes. Leaves and flowers are complex above-ground organs initiated at the Shoot Apical Meristem (SAM) (Figure 1). In *Arabidopsis thaliana* decades of studies on SAM gene expression has identified most of its regulators. An interplay between SAM transcription factors and regulatory genes contributes to regular positioning of leaves and flowers around the stem, i.e. phyllotactic patterns. Some of these genes also contribute to the overall organization of the SAM in different regions and layers (Tian et al. 2019). By observing morphogen distributions at different developmental stages, we now have an almost complete map of *A. thaliana* genetic markers in the apex (Carraro et al. 2006). Still, it is not clear how gene expression at the cellular level leads to morphological changes at the organ level.

The organization of the SAM is conserved in vegetative and reproductive stages. The central zone (CZ) of the meristem contains a small, stable pool of stem cells which are slowly growing and dividing (Steeves and Sussex 1989) (Figure 1). As the SAM pushes up, the initiated cells from the central zone later form a ring of cells called peripheral zone (PZ), where growth and proliferation is faster. Organ primordia are

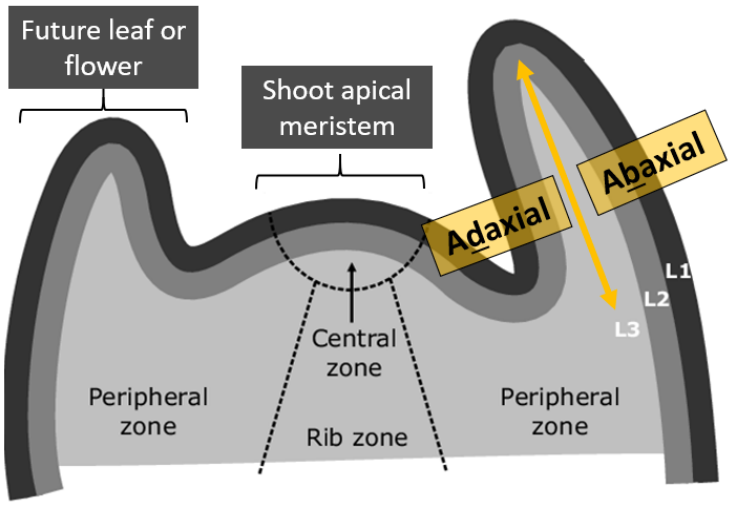

Figure 1: Structure of the shoot apical meristem, longitudinal cross section. *The SAM is stem cell niche, perpetuated at the apex of the plant. Organ primordia (i.e. future leaves or flowers) are delineated from the meristem by a crease of slow-dividing and slow-expanding cells. In the case of the flower, it is formed between a cryptic bract (leaf-like structure) and the SAM peripheral zone. L1: epidermis, important for phyllotaxis (organ positioning). L3 is formed of the Peripheral Zone (PZ) and Rib zone, with cells dividing in all directions. Cell fate differs in* primordia *(future leaf or flower) depending if the cell faces the meristem center (adaxial side) or is away from it (abaxial side of primordia).*

initiated only from the cells located in the PZ, while the CZ always conserves a stem cell identity. The SAM is also organized in successive clonally distinct layers, each with an assumed specific function in development (Figure 1). The outermost, epidermal layer (L1 layer) was shown to be important for organ patterning and initiation (Kierzkowski et al. 2013). In most higher plants, cell divisions in the L1 and L2 layers are mostly anticlinal, (i.e. perpendicular to the surface of the SAM) causing their cell lineages to remain clonally distinct. Both layers form so called tunica, sheltering internal tissues. In the L3 layer, also called corpus, the orientation of divisions is more random (Steeves and Sussex, 1989; Lyndon, 1998). The L3 and subsequent layers contribute to the development of procambium (future vascular tissue) and other stem structural tissues (Benková et al. 2003; Dorota Kwiatkowska and Dumais 2003; Soyars, James, and Nimchuk 2016) (Figure 1).

While functionally and morphologically distinct, both leaves and flowers share a common evolutionary ancestor and important genetic regulators. An overexpression of the flower meristem identity gene LEAFY can cause early flowering in vegetative meristem (Parcy et al. 1998). These organs are also morphologically similar at their initiation, as both structures arise by bulging out of the surface in the peripheral zone. However, flowers emerge at the boundary zone between the SAM periphery and a bract, a leaf-like organ formed at the flower bud. (Dorota Kwiatkowska and Routier-Kierzkowska 2009). While the bract was initially thought to be nonexistent in the *Brassicaceae* genus, further studies demonstrated that it is aborted early in development due to change in the local distribution pattern of genetic markers (Long and Barton, 2000).

While both leaf and flower primordia have comparable overall organization, the obvious morphological differences between leaves and flowers suggest that cell dynamics (i.e. cell growth and division patterns) at early primordia might be significantly different. So far, most studies describe cell division, rarely cell expansion, and are limited to the epidermis, leading to contradicting information as to whether cell expansion or cell division underlies organ initiation in the SAM. In some of those studies (D. Kwiatkowska 2004a; Long and Kathryn Barton 2000; Vaughan 1955), both leaf and flower initiation are marked by a strong surge in cell expansion in the L1 layer, and it is also accompanied by an increase in cell number. This increase in cell proliferation is considered the first sign of organ initiation. In leaves, periclinal divisions in the L2 layer have been observed prior to organ outgrowth, first on the abaxial side of the growing leaf (Vaughan 1955). In flowers, periclinal divisions in the L3 layers have been proposed to cause primordia initiation (Vaughan 1955). Reddy and co-workers hypothesized that cells from the PZ that divide parallel to the primordia outgrowth axis signal organ initiation, at least in the first two layer of the SAM

surface (Reddy et al. 2004). In contrast, a study by Grandjean and co-workers indicates that cell division is not required for primordial outgrowth in the earliest stages of organ development (Grandjean et al. 2004a). In most of those studies, cell expansion analysis was technically challenging or impossible, especially in inner layers. Most provide a clear depiction of the cell dynamics in L1, yet do not quantify growth in inner layers, and thus fail to present a complete picture of primordia initiation.

In this study, I present in detail a complete pipeline to study 3D cell dynamics in plants. Using this methodology, I show the first complete four-dimensional quantitative analysis of both leaf and flower initiation at cellular resolution. My data suggest that changes in cell expansion, rather than cell division, are the first marker of organ outgrowth. I also show that the main difference between leaf and flower primordium is a specific spatio-temporal distribution of cellular growth at their very early stages of development.

Materials and Methods

Plant material and growth conditions

Arabidopsis thaliana plants carrying pAtUBQ10::myr:YFP transgene in a standard *Columbia* background used in this study were described previously (Yang et al. 2016). Plants were grown on soil in a growth chamber under long day conditions (16h hours of day, ~ 95 µmoles $m^{-2}s^{-1}$ irradiance, 50 – 80% humidity, 23°C). For time-lapse experiments, 14 (for leaf initiation) or 21 (for flower initiation) days-old soil-grown plants were dissected and transferred to ½ MS (Murashige-Skoog) medium with vitamins (Fisher Scientific) and supplemented with 1% sucrose, 1,5% plant agar (Fisher Scientific), and 0,1% PPM (Plant Cell Technology) and cultured under long day conditions (22-23°C, ~ 80 µmol.m^{-2}.s^{-1} irradiance, 16 hours of illumination).

Microscopy

Confocal imaging was performed with Zeiss LSM800 upright laser-scanning microscope, equipped with long working-distance water immersion objective (AP 40x/0.8). The YFP fluorescence was excited using diode laser at 514 nm and the emission was collected with a Gallium Arsenide Phosphide (GaAsP) detectors at 520-550 nm. Data were collected as 16-bits images. Images were taken at 512x512 resolution,

with 0.5 µm distance in Z-dimension, and no averaging to minimalize imaging stress. Four flower and leaf series imaged for 48-82 hours are presented in this study. Image collection was done at 12 hours interval.

Growth tracking

Time-lapse imaging with 12 h intervals was performed using a modified protocol described previously (Kierzkowski et al. 2012). Briefly, 14-day-old (leaf initiation) or 21-day-old (flower initiation) samples mounted on media were carefully dissected to uncover meristems (without damaging hypocotyl nor root system). Dissected plants were entirely immersed in a 0.1% PPM water solution for at least ten minutes before each imaging. Between imaging, the samples were carefully dried from excess water and and cultures on the same MS medium in the growth cabinet as described above. Here, we define growth as the ratio of the total volume (or surface) of a cell progeny over the initial volume of the cell, $Volume\ of\ cell\ A\ at\ T_{final}\ Volume\ of\ cell\ A\ at\ T_{initial}$. Growth depends on the time interval (T) being considered. The volume of the cell at T_{final} does not depend on division.

Image analysis

Image analysis and processing were performed using MorphoGraphX (Barbier de Reuille et al. 2015) and custom-made Python scripts available at:

https://drive.google.com/drive/folders/14M5rZkqn6ncqkelxdYGZKLXOhJc7lH9t?usp=sharing

Statistical analysis

All statistical tests were implemented in custom Python scripts. To quantify the error caused by manual segmentation, the normality of cell size distribution frequency was evaluated using a Kolmogorov-Smirnov test. Variance equality between the sets was tested with a Barlett's test. The same tests were used to evaluate the significance of growth values distributions between cell layers of flower and leaf primordia.

Results

1) Confocal time-lapse imaging

To obtain complete cell lineage information of leaf and flower primordia, I imaged SAM samples at 12-hour intervals and obtained whole series of confocal 3D images. While confocal imaging has improved to

be less detrimental to samples, it is still recommended to minimize sample exposure to laser. Laser

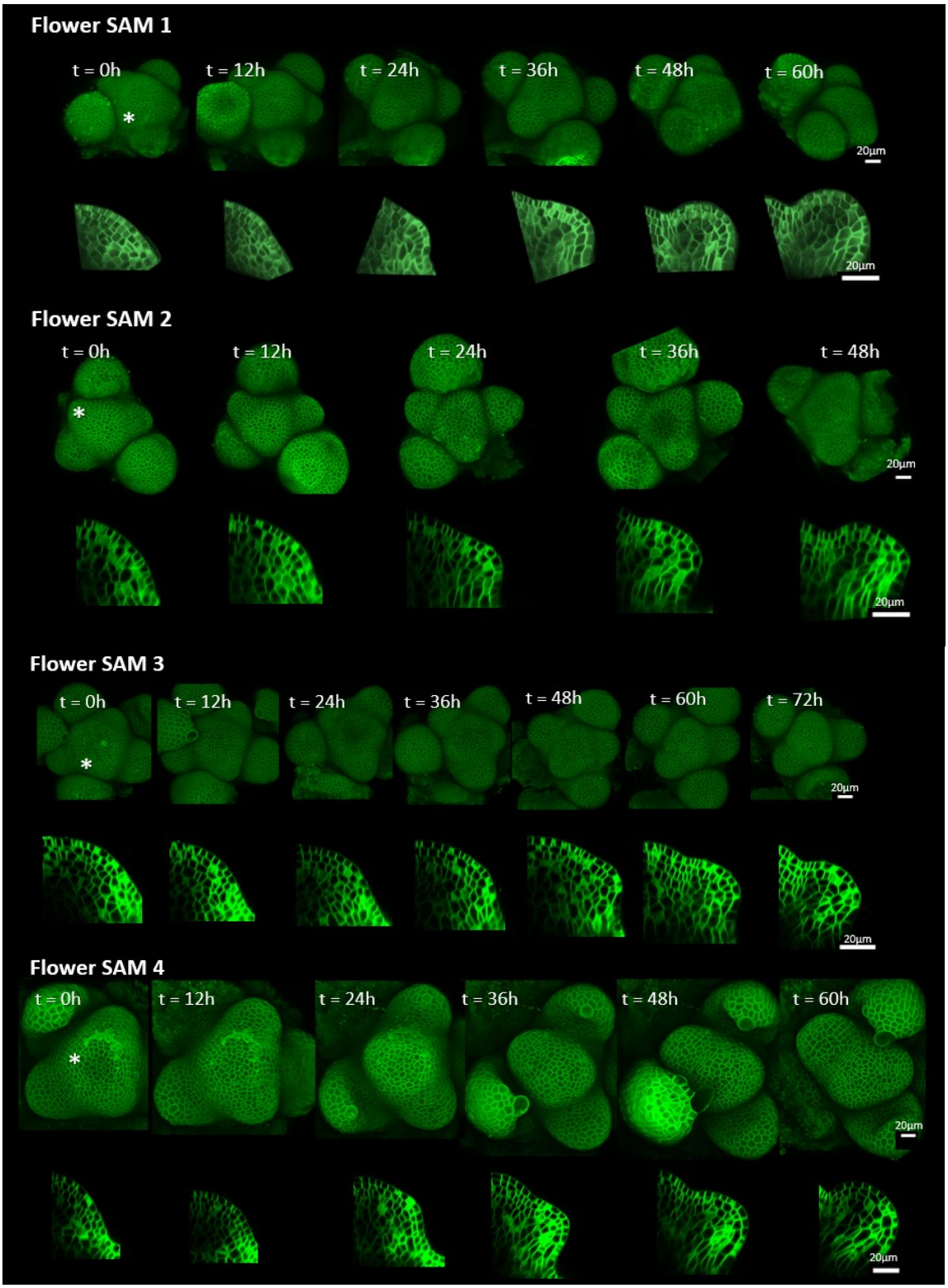

Figure 9 : Confocal series of the inflorescence SAMs used. *Longitudinal cross-sections of the targeted flower primordium are shown. Asterisks mark the position of the targeted primordia.*

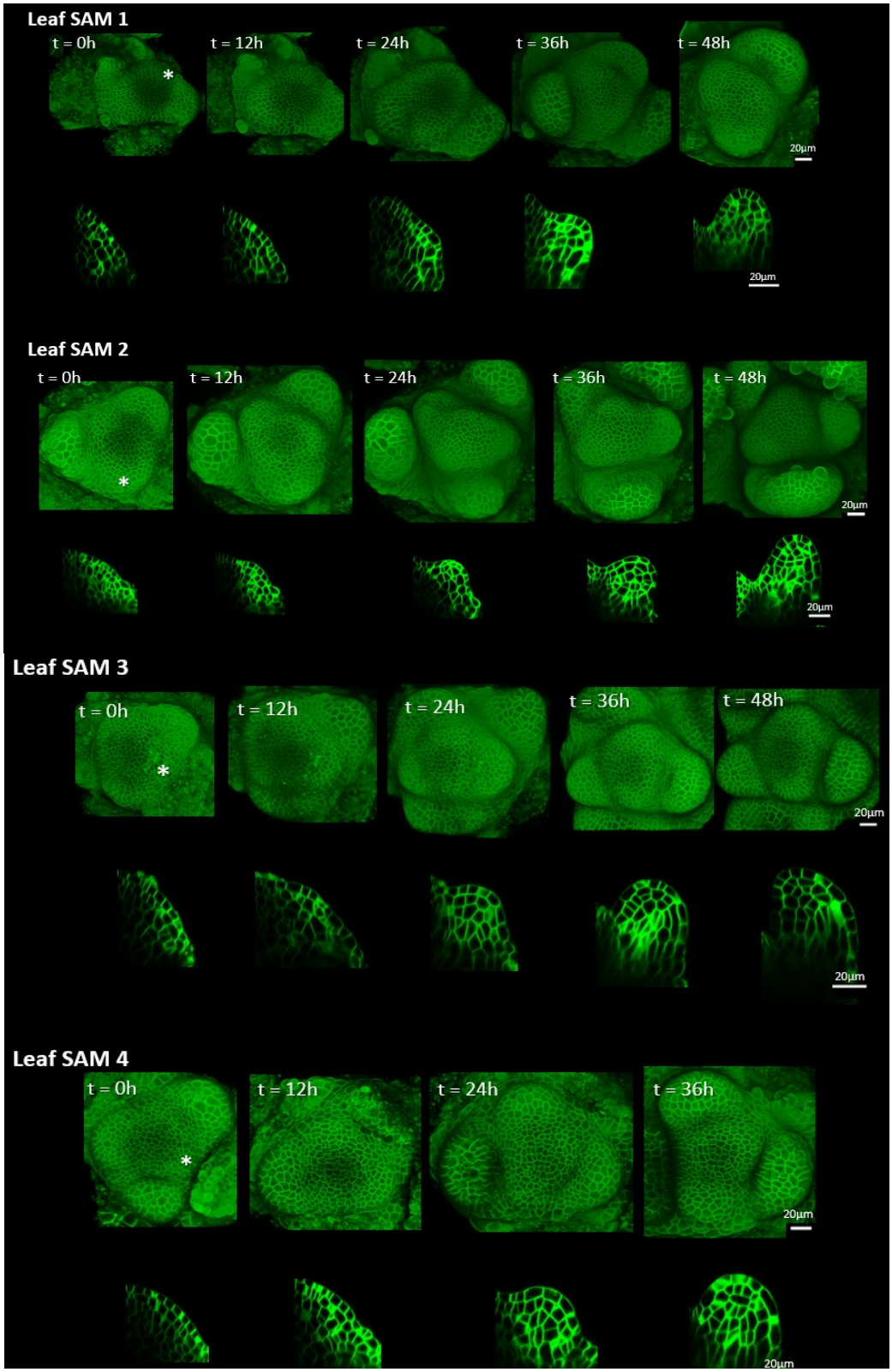

Figure 16: Confocal series of the vegetative SAMs used. *Longitudinal cross-sections of the targeted leaf primordium are shown. Asterisks mark the position of the targeted primordia.*

exposure is a cause of stress and can affect plant development. On the other hand, following cell lineages

requires to observe cells at frequent time intervals, to properly monitor division and growth of each cell. A 12-hour time interval was proven a good compromise, as it allows regular observations without significantly affecting cellular behavior. Initiating organs were followed over 48 to 84 hours. Based on the image quality, I selected time-lapse series of four flower primordia and four leaf primordia (Figures 2 and 3). Each series represented a biological replicate, i.e. a different organ on a different plant.

The following criteria were used to evaluate the series quality. First, the signal emitted from the plasma membrane fluorescent marker was sufficiently strong to allow a clear delimitation of each cell in all targeted layers and for each time point. Secondly, the samples selected displayed a growth rate of at least one plastochron (i.e. time interval between two successive organ initiation events) per 24 hours. Lastly, I made sure that the CZ and PZ of the SAM samples were kept intact all along the experiments. While it has previously been shown that ablation of the CZ does not prevent primordia growth (Grandjean et al. 2004b), ablation at the SAM redirect auxin flux (Smith et al. 2006) and thus affect growth. Overall, growth of most of the samples matches with what can be found in the literature (Kwiatkowska and Dumais 2003); (Kwiatkowska 2004b; Jones et al. 2017; Willis et al. 2016).

2) A 3D segmentation pipeline in MorphoGraphX for analysis of SAM primordia

To track cells over time, I used MorphoGraphX (Barbier de Reuille et al. 2015) to extract the 3D shape of each cell from 3D confocal images of the emerging primordia. The software was primarily designed to analyse cell dynamics (cell division, cell expansion, lineage tracking) on curved surfaces, which is very similar to analysing 2D data. However, cell dynamics is more challenging to analyse in three dimensions, since the cells are surrounded by neighbors from the same layers as well from the layers beneath and above. I therefore created my own protocols using MorphoGraphX and custom Python scripts to accurately delimitate the epidermal and internal layers in the shoot apex (Figure 4). This pipeline is currently used by other members of the lab to analyse other type of organs with complex 3D geometry.

Confocal data (i.e. 3D image stacks, Figure 4) from each time point are analyzed separately at first. In order to limit computation time, I chose a region of interest to segment cell in 3D (in red; Figure 4, step 2). Segmented cells are represented by a closed surface, which is a triangular mesh. The mesh is used to store data such as cell label (a unique identification number) or compute quantities such a cell volume. Once

3D cell mesh is created, it is possible to precisely identify from which layer and part of the SAM cells are initiated (Figure 4, step 3). Finally, once the cells have been segmented for each confocal stack of the time series, cell labels can be associated from one timepoint to the next (Figure 4, step 4). The lineage tracking is done manually, by comparing the geometry and the contacts between cells in two consecutive timepoints. For example, each cell at the time point t = 24h will be assigned a mother cell from the time point t = 12h. One mother cell at t = 12h can have several daughter cells at t = 24h. Assigning mother cells allows identification of cell growth, proliferation or direction of growth between two points of a series. Once consecutive timepoints from the whole series have been compared, the complete cell lineage

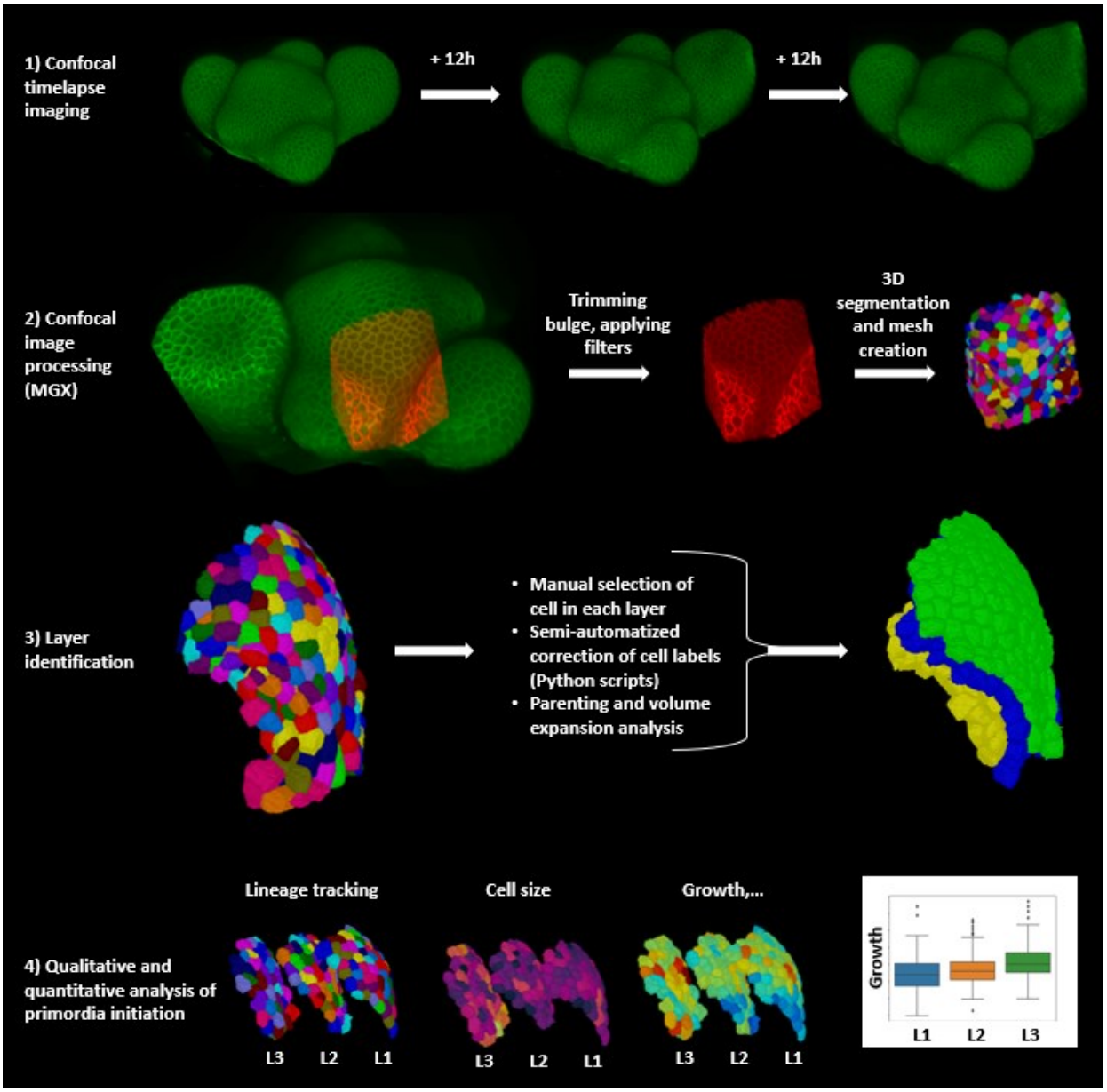

Figure 4: A 3D segmentation pipeline. *Description in the main text.*

history can be retrieved (See *Comparison of cell dynamics between leaf and flower during primordia initiation,* Figure 15). It is important to note that the full pipeline of analysis I am proposing here can be apply to any other plant organ.

Detailed description of the 3D analysis pipeline

The basic procedures related to the usage of MorphoGraphX are not detailed in this section, as they have been extensively explained in the MorphoGraphX guidelines (Strauss et al., 2019). Additional help can be found in the MGXUserManual.pdf presented in the Help section of the software.

All the scripts used in the pipeline rely on a pre-defined folder organization and exact file nomenclature[1]. Users should refer to the directory tree TEST_DIR to see how to organize their data. This directory contains a fully segmented series of wild type shoot apical meristem (WT SAM). An accompanying ReadMe file present the function and usage of the scripts.

a) 3D segmentation

The original confocal image can be quite large compared to the structure user wants to segment. Applying the 3D segmentations algorithms can also be demanding in computer processing power. Consequently, we recommend to first trim the original stack as much as possible to isolate the structure of interest (Figure 5) and save the resulting trimmed stack.

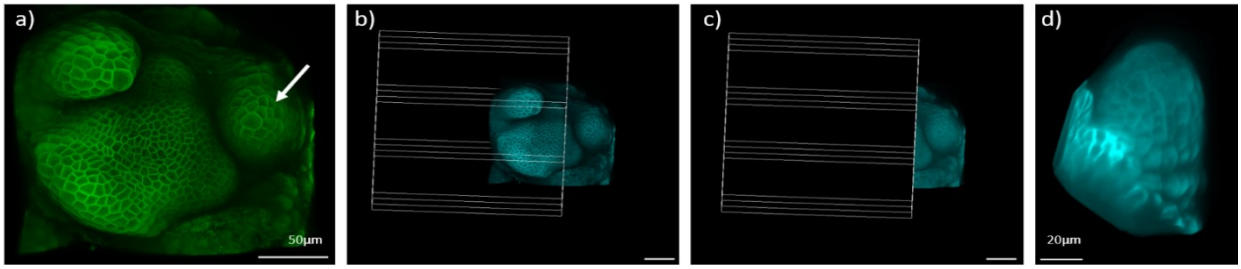

Figure 5: Trimming structure with clipping tools and Voxel edit. *a) A full shoot apical meristem from an* A. thaliana *plant. The arrow points to the target structure to be analyzed (leaf primordium). b) and c) show how to use the clipping tool to for tailored trimming. d) Resulting trimmed stack. It is better to have more cells at the periphery of the bulge/structure than needed, as cells with incomplete cell walls will be lost during segmentation (see Figure 3).*

[1] Scripts are available here:
https://drive.google.com/drive/folders/14M5rZkqn6ncqkelxdYGZKLXOhJc7lH9t?usp=sharing.
For file organization, see TREE_EXAMPLE directory here:
https://drive.google.com/drive/folders/1CJpTbvq5Na4r64FG5mWlOd5A2SHbaGiQ?usp=sharing.

Next, launch the script `Create_3D_stack.py`. The script automatizes some of the processes required for 3D segmentation and is designed to save considerable amount of time. The output is a 3D stack and mesh (with a size heatmap) from the input trimmed stack.

First, the script applies custom filters to the trimmed stack to remove noise. I propose a combination of three filters (in 'Stack > Filters'): 'Gaussian Blur' (0.3, 0.3, 0.3); 'Normalize Stack' (5, 5, 5, 0.3, 0.3, 0.3, 10000, 7) and 'Top hat' (10, 10, 10, No). The parameters of those filters can be adjusted for better accuracy. If the quality of the confocal stack is good, the 'Gaussian Blur' filter should be sufficient.

Next, the script generates a 3D segmented stack using the 'Insight Segmentation and Registration Toolkit' ('ITK') automatic segmentation algorithm (Barbier de Reuille et al., 2015). The resulting 3D stack is used to create a 3D mesh, obtained by running 'Mesh>Creation>Marching Cubes 3D'. The default parameters in the script are as follow:

- Cube size (the smaller the cube size, the higher the mesh resolution): 0,5
- Min voxels : 0
- Smooth Passes: 1

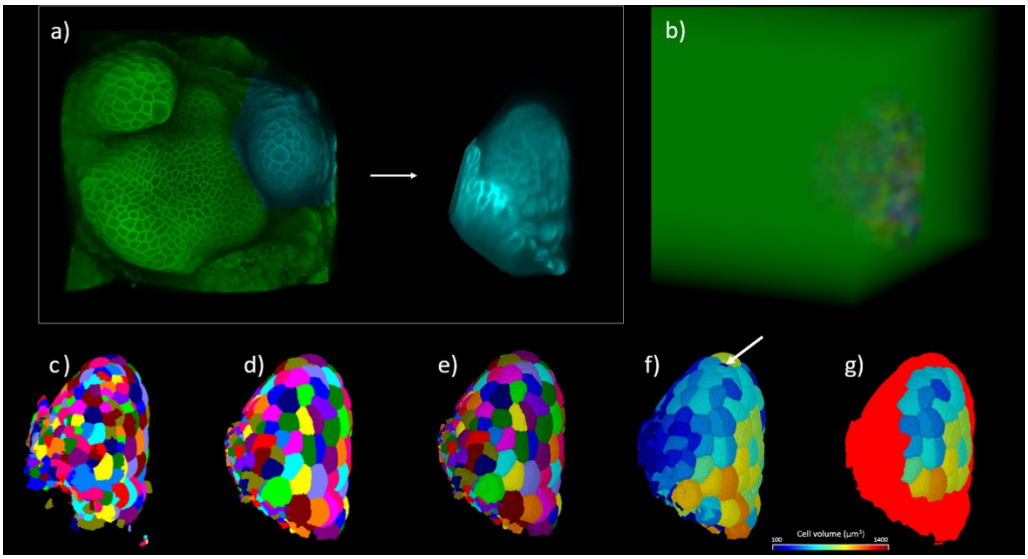

Figure 6: From trimmed stack to 3D mesh. *a) Once the stack has been trimmed and filters applied, run the 'ITK' segmentation algorithm. b) The 'ITK' process creates a 3D stack with a large "cell" (green shadow here) surrounding the stack. This cell label can be removed by running 'Stack>Segmentation>Erase at Border', or by replacing the label by 0 (with the 'Fill stack label' tool). c) The 3D stack can be over or under segmented. In both cases it is possible to either start over with a different filter and/or 'ITK' level combination, or, as it was done here, d) to fix the errors right away (See Troubleshooting – Cells are over segmented section for details).e) With the 'Marching 3D' process, the 3D stack is converted into a 3D mesh. f) Generating a cell size heatmap from the mesh allows to spot errors not readily observable from the stack or mesh. Here, the arrow points an aberrantly small "cell", resulting from over segmentation of the 3D stack. g) Once all errors have been corrected, use the 'Selection' and 'Inverse selection' tools to manually save the cells of interest.*

- Label (0 is default for the total stack; give a stack label number to apply to specific cell): 0

Once all the modules have been run, `Create_3D_stack.py` saves the options used in a separate .info file. Unless there are obvious errors in segmentation (See *Cells are Over segmented* section), the resulting 3D stack **must not** be modified later, as labels of 3D stack are identical to the ones of the 3D mesh.

b) Select layers of interest

Select cells manually from mesh (Figure 6f and g); refer to the MGXManual.pdf for more details). Save separately the selected cells 3D mesh, its complement (using Inverse selection command) and its label list (Use 'Mesh>Heatmap>Heat Map Classic' to generate a label list).

NB: Label lists are important to regenerate the mesh from the original 3D stack and should be kept. All modifications to the 3D stack and 3D mesh must be reflected in those lists.

Repeat the process on the complement mesh for the next layer(s) needed for analysis. Once all desired layers have been selected and stored, discard the complement meshes, except for the last layer complement mesh (this layer will bear potentially missing cells from the last saved layer and should be kept in case future corrections are needed).

At this point you should have:

- The fixed 3D stack (.tif)
- The meshes of target layers and the last complement (.mgxm)
- The corresponding label lists (.csv) of those meshes

c) Correcting layer attribution

Cells may have been wrongly attributed to a layer (example in Figure 7). Start by loading the problematic layer (e.g. L2 layer) in the first Stack and its adjacent layer (e.g. L3 layer) in the second Stack. Open the script `Correct_Layer_Attribution.py` on the side and write the labels that needs to be exchanged between layers. The script will automatically correct the 3D meshes and label lists of both layers (Table T1, `Correct_Layer_Attribution.py`).

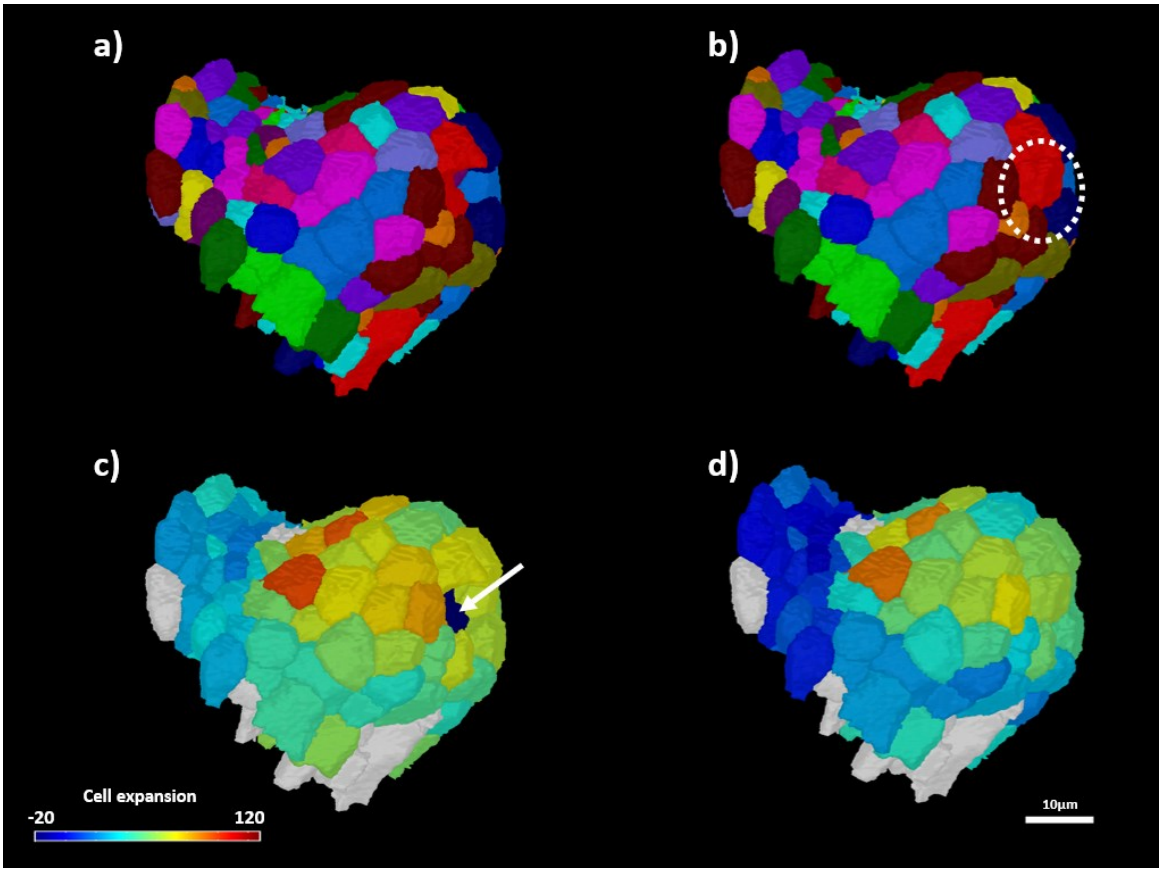

Figure 7: Correcting cell attribution. *(a) and (b) show a layer mesh before (a) and after (b) layer attribution correction. (c) and (d) are the corresponding growth heatmaps. In (c) the heatmap reveals a daughter cell (arrow) with an aberrant growth value. After running the script, the missing daughter cell is added from an above layer, and the parent mother cell layer is added (b, dotted circle).*

d) Assigning mother and daughter cells between consecutive time-points (parenting)

Once the cells are segmented for each time point in the series, we can determine how cells are related to each other between timepoints. This procedure is called “parenting” in MorphoGraphX. It consists in manually examining the cell shapes and connectivity to find which cells in the first time-point divided in the second time-point and assign mother cells to their corresponding daughter cells. The tools used for parenting in 3D are similar to the ones used on curved surfaces (see Barbier de Reuille et al. 2015). Using the ‘Blend’ tool on the parent mesh to easily observe and compare both parent and daughter cells in 3D (Figure 8).

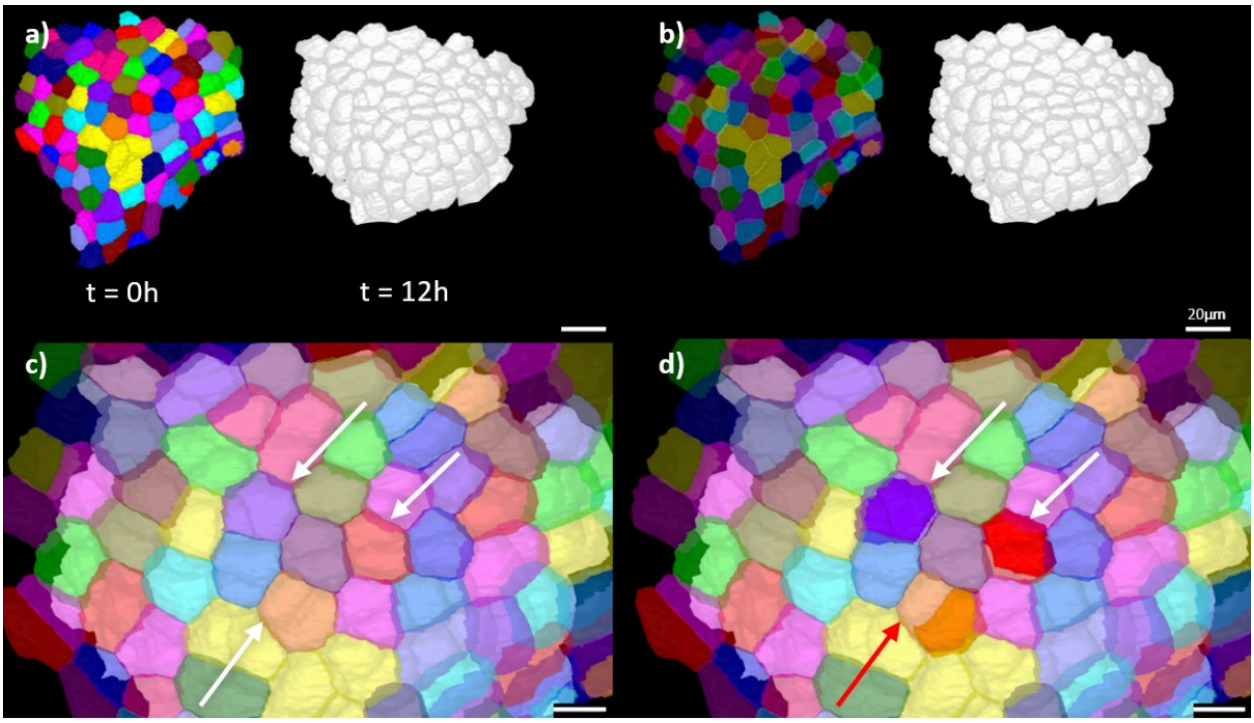

Figure 8: Parenting a 3D mesh. *a) The labelled layer (with colors) is from an earlier timepoint and the unlabelled one (white mesh) is from a confocal stack obtained 12 hours later. b) Aplying the 'Blend' tool to the first mesh gives it transparancy while still allowing the mesh to be manipulated. Thus the 'Blend' tool can be used to superimpose both meshes and ease up the parenting process. c) Superimposed meshes. d) By using the 'Grab' tool, we can attribute parents. Here, both the purple and red parents (white arrows) have divided in two cells, and have been attributed. The orange parent label (red arrow) is in the process of being attributed.*

While parenting the epidermal layer is straightforward, parenting subepidermal layers requires additional precautions. Since divisions can happen in any direction in those layers, it is important to look at the mesh from all angles (e.g. by looking from both front and bottom sides of the layer) to complete parenting. Even then, cells can divide within the layers and thus will not be visible from either side of the mesh (Figure 9). In such situation, it is possible to combine the 'Fill label' and the clipping tools to localize all cell progeny: the clipping tool will make inner cells visible without altering the mesh; then we can select the parent label, and fill the daughter cell with this label (Figure 9).

Once all parents have been identified between two timepoints, it is important to analyze growth, in order to detect errors when assigning mother and daughter cells, with the process 'Mesh > HeatMap > Analysis > Heatmap Classic'. Again, we define growth as the ratio of the total volume (or surface) of a cell progeny over the initial volume of the cell, $\frac{Volume\ of\ cell\ A\ at\ T_{final}}{Volume\ of\ cell\ A\ at\ T_{initial}}$. Growth depends on the time interval (T) being considered. The volume of the cell at T_{final} does not depend on division. Missing /additional cells in lineage

are easily spotted on the heatmap (Figure 10). It is important to fix those errors before moving to the next layer.

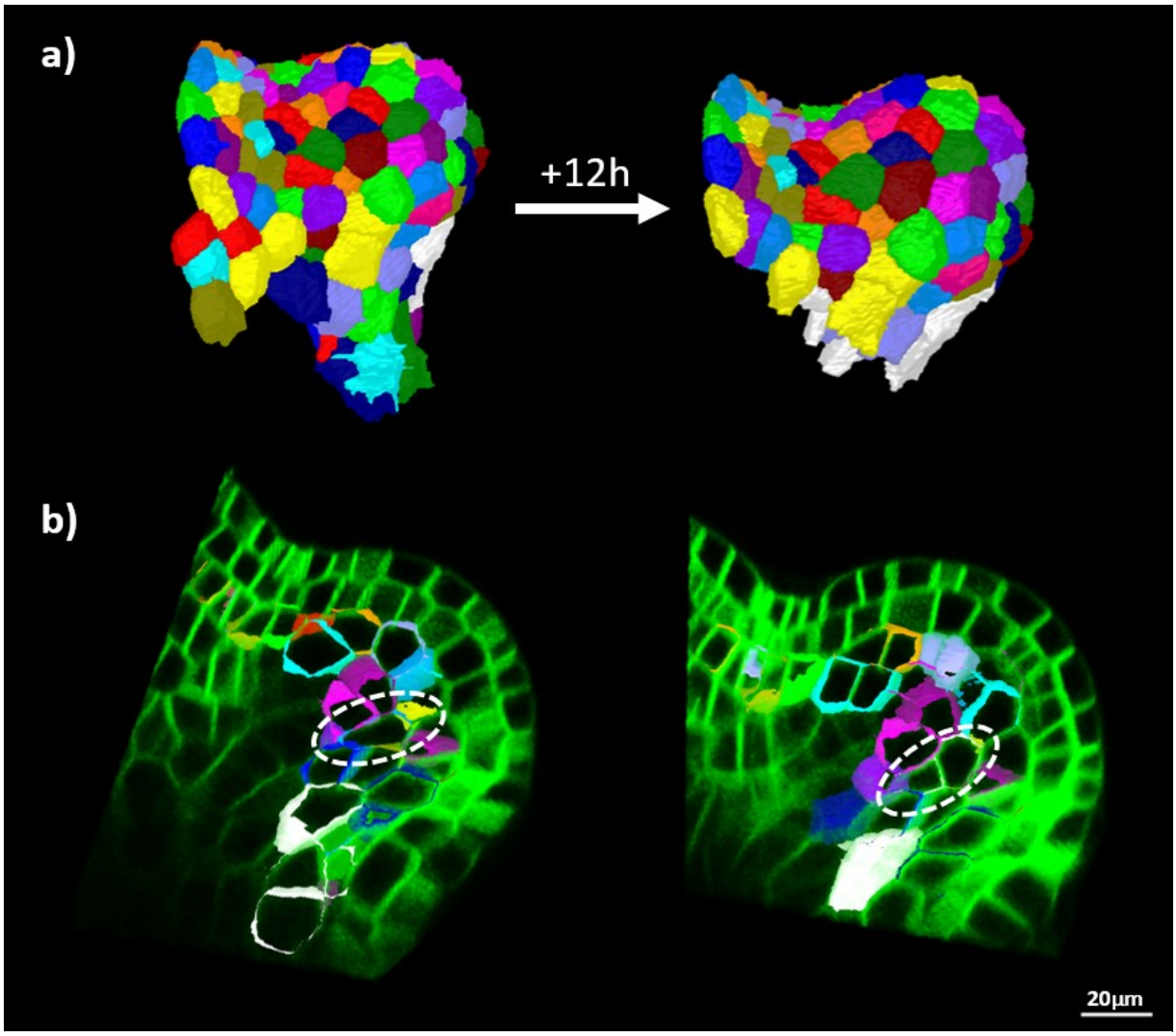

Figure 9: Tracking cells in deeper layers. *a) Parenting done between two 3D meshes extracted from the L3 layer of a developing primordium. This was done as explained in Figure 4. b) Longitudinal cross section of the two meshes reveals that a cell (blue label in circle, left image) has become embedded within the mesh. At the next timepoint, this cell has divided in two daughter cells (circle, right image). This illustrates how periclinal divisions happening in subepidermal layers makes it harder to track cell lineages.*

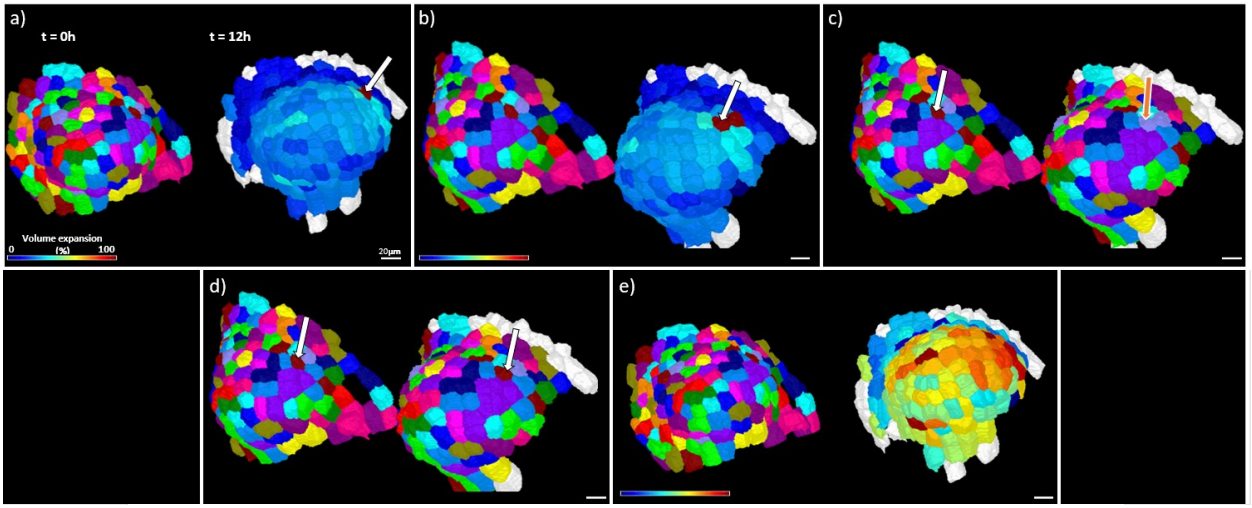

Figure 10: Growth analysis and fixing parenting errors. *a) and b) two orientations of the same structure at two time points. Growth heatmap between the two time points shows two cells that appear to have expanded abnormally (in red). c) Switching to parent label view, we can see that the cell in red (white arrow) was not assigned any daughter cell, and the purple cell next to it has two daughter labels instead (orange arrow). After correcting the parenting (d), and running a new growth heatmap (e), we see that the cell growth distribution is much smoother (i.e. no more than ~20% variation in growth between two cells of a same area), homogenous than in (a) (i.e. there are no aberrant growth difference between adjacent cells in a same region).*

Once all corrections have been done, run the 'Heat Map Classic' analyzing process again: the heatmap should display a "smooth" repartition of growth (Figure 10e). If the heatmap is still not smooth, some cells might have been missed while parenting: using the clipping tool, scan the mesh again for unlabeled cells, until maximal homogeneity is attained. It is also possible that cells are missing and are in another layer (See section *Correcting layer attribution*).

e) Troubleshooting

The next section describes common segmentation errors and how to fix them. It is good practice to first scan the cell size distribution heatmap obtained after creating the first mesh to spot errors early.

i) Cells are missing from the 3D stack

Low confocal signal in the cell walls will result in gaps in the 3D stack (Figure 11). Those gaps will appear more often at the epidermal layer but can also occur within the stack.

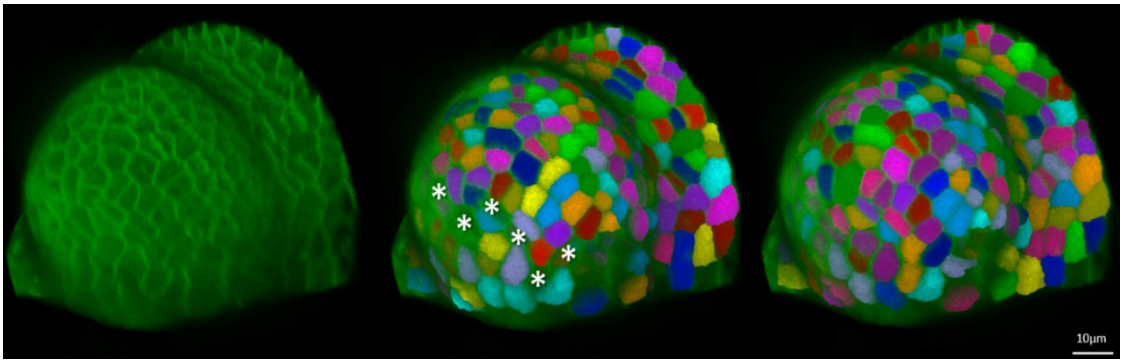

Figure 11: Poor signal and 3D stack. *Lowering the 'ITK' threshold level from 1500 (right) to 800 (middle) results in more cells in 3D stack. Asterisks (*) shows the gaps (missing labels) that have been corrected in the new 3D stack. Notice how the stack labels have all been changed (different labels colors).*

When this happens, it is better to try to recreate the entire 3D stack, reducing the 'ITK' threshold and adjusting filters. However, this will change all the labels, which is not desirable if other layers from the stack have already been analyzed. Another possibility that would prevent starting the procedure from the beginning is to:

- Create a new 3D stack with only the missing labels from the first 3D saved stack
- Use the 'Stack>Multistack>Combine Stacks' (Method Max) to combine the saved stack and the missing cell stack
- Use this new final stack to recreate the mesh

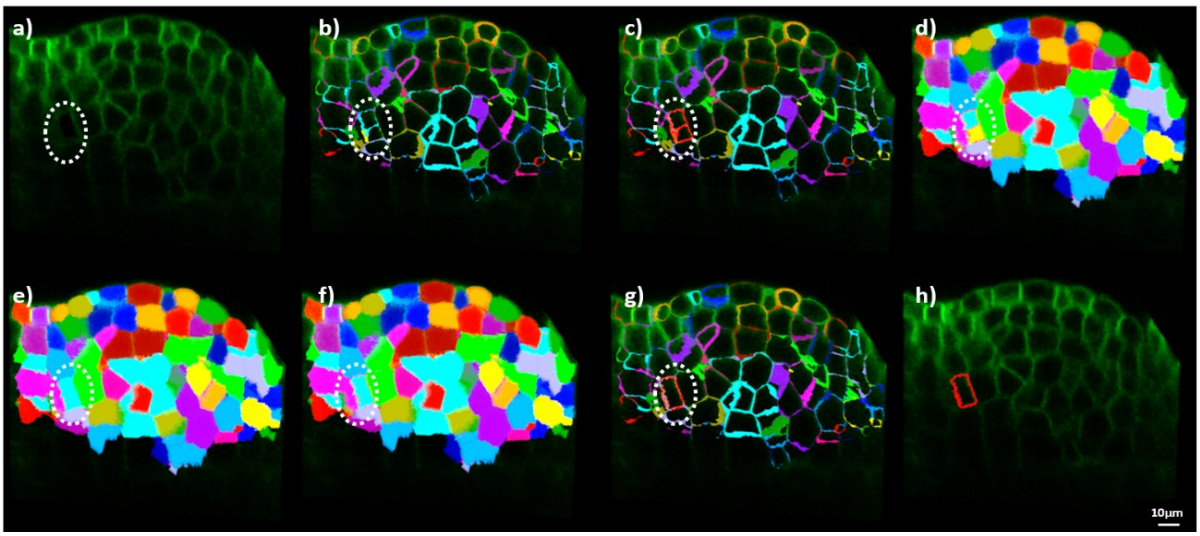

Figure 12: Fixing over segmentation. *a) Longitudinal cross section of a primordium confocal stack. b) Longitudinal cross section of confocal stack and generated 3D mesh. The cell shown in a) (circle) has been over segmented into two cells (blue and yellow labels, circle). c) To correct the error, first select the two cells (they will appear in red). d) Load the 3D stack in the 'Work Stack' in MGX. e) Run 'Stack>Segmentation>Join Regions': it will fuse the 3D stack labels in one. f) Select the new stack label and run 'Mesh>Creation>Marching Cubes 3D' for this new label only. Save the corrected stack and mesh. g) the new label (circled, also selected in red in h) now shows the correct delimitation.*

Make sure the missing cell stack has different labels than the saved stack by checking the saved stack label list prior the combining stacks.

ii) Cells are Over segmented

I implemented a script that automatically corrects over segmentation errors (Table T1, `Correct_Oversegmentation.py`). It can also be done manually, as described in the following section.

Use 'Stack>Segmentation>Join Regions' to fuse cells of the 3D mesh, delete the combined mesh, then run 'Mesh>Creation>Marching Cubes 3D' **only** for the resulting label (See `Create_3D_stack.py` for ideal parameters) (Figure 12).

Make sure to update the label lists as well and to recreate the affected layer as needed (Use the `Make_3D_mesh.py` script).

NB: Additional over segmentation errors are often found later in deeper layers. It is good practice to scan trimmed stack and 3D mesh with size heatmap with the clipping tool, as it makes over segmentation errors obvious (Figure 13).

It is important, when using 'Join Regions', to make sure that the 3D stack is loaded in the 'Work Stack'. Also, make sure to save both the 3D stack and new corresponding mesh.

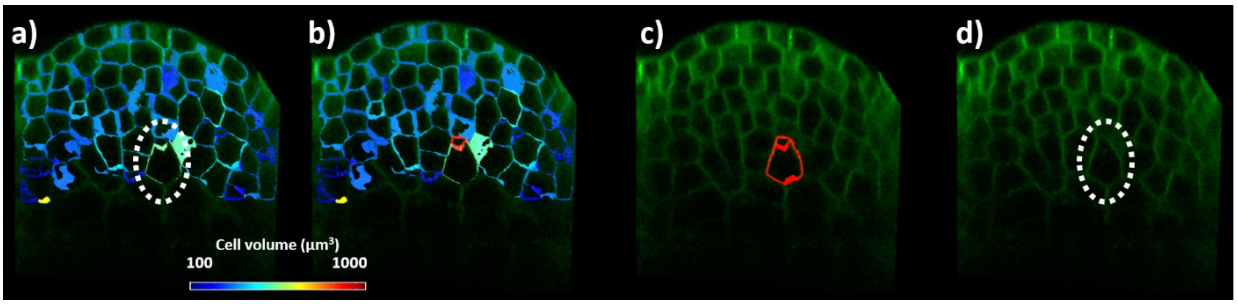

Figure 13: Spotting over segmented cells with cell size heatmap and clipping tool. *a) Cross section of a confocal stack and corresponding stack with size heatmap. b) An abnormally small cell is selected (in red). c) The small cell and its partner (both in red) are actually the same cell, as proven by the original confocal stack in (d). d) Confocal stack cross-section with the real cell position circled.*

iii) Cells are under segmented

When there are aberrantly big cells (Figure 14a-b), reduce the threshold level of the 'ITK' segmentation to generate a new 3D stack. It is better to start off with an over segmented 3D stack since it is easier to fix.

If already advanced in the analysis (e.g. the epidermal layer and adjacent subepidermal layer have already been fully labelled and cells parented at this timepoint), it is not desirable to recreate a new 3D stack, as all labels will be changed. Instead, it is possible to (1) delete those problematic cells from the 3D stack first; (2) create and save a new 3D stack with those cells separately, (3) combine both stacks ('Stack>Multistack>Combine Stacks'(Method Max)) and re-create the 3D mesh (Figure 14).

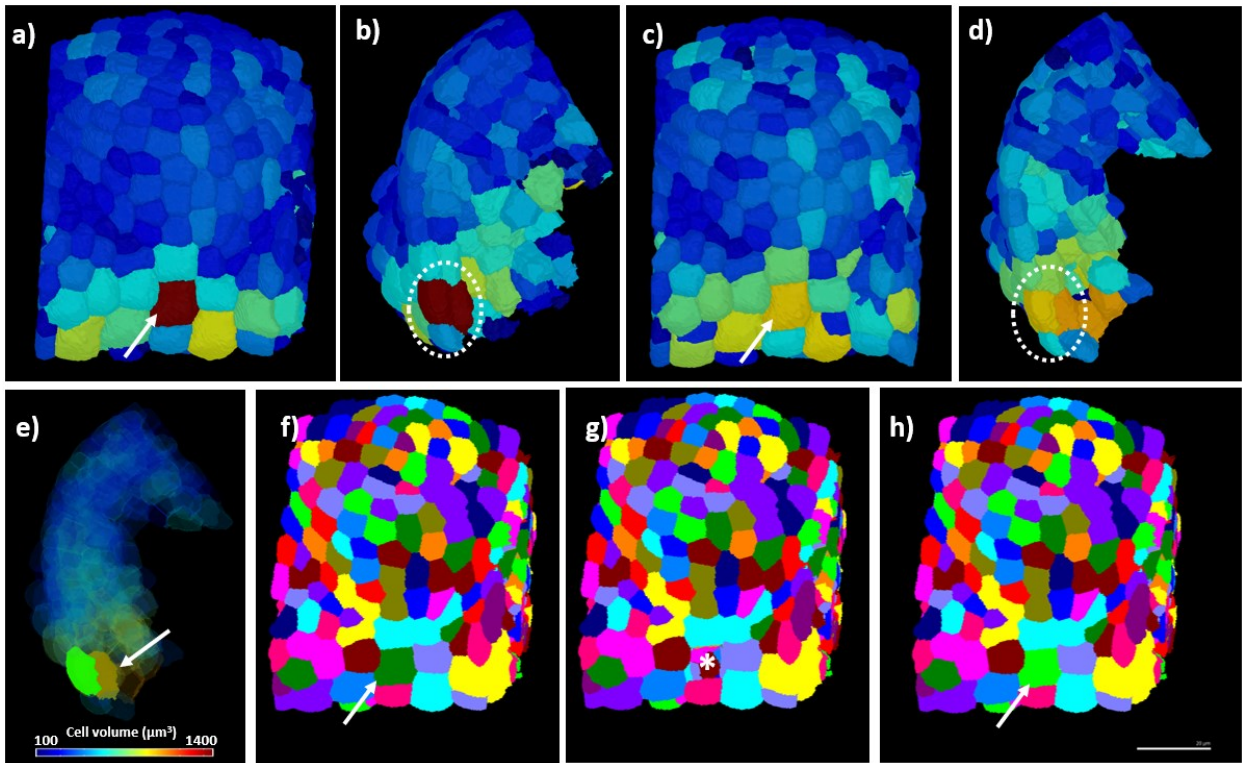

Figure 14: Fixing under segmentation. *a) Generating the growth heatmap in this mesh revealed an aberrantly large volume (red cell). b) Cross section view of the mesh reveals this cell extends through both the epidermal and subepidermal layers. (c) and (d) New cell size heatmap from new mesh after correction (front and side view). e) The first step in correcting under segmentation is to create a corrected 3D stack from the original confocal stack. Here, the corrected stack is made of two cells (in light green and olive, arrow) The 'Blend' tool is used to show the correction in the mesh. f) First, load the saved 3D stack initially created, with the problematic under segmented cell (dark green, arrow). Load it in the 'Work Stack' position. g) Delete the problematic cell (*) from the saved stack. h) Load the corrected stack (with the two new cells) in the 'Main Stack' position. Since they are from the same original confocal stack, they will overlap perfectly. Run the 'Stack>Multistack>Combine Stack' (Method Max) process to fuse both stacks in one. Save it, then re-create 3D mesh and a new cell size heatmap to verify correction.*

f) Preparation for analysis

Once the layers of the organ have been separately curated, some additional operations must be done to create the final mesh. I wrote specific scripts to combine layers of interest (Table T1) or to create a specific display (e.g. Figure 4, Step 4). Details can be found in the "Readme" file.

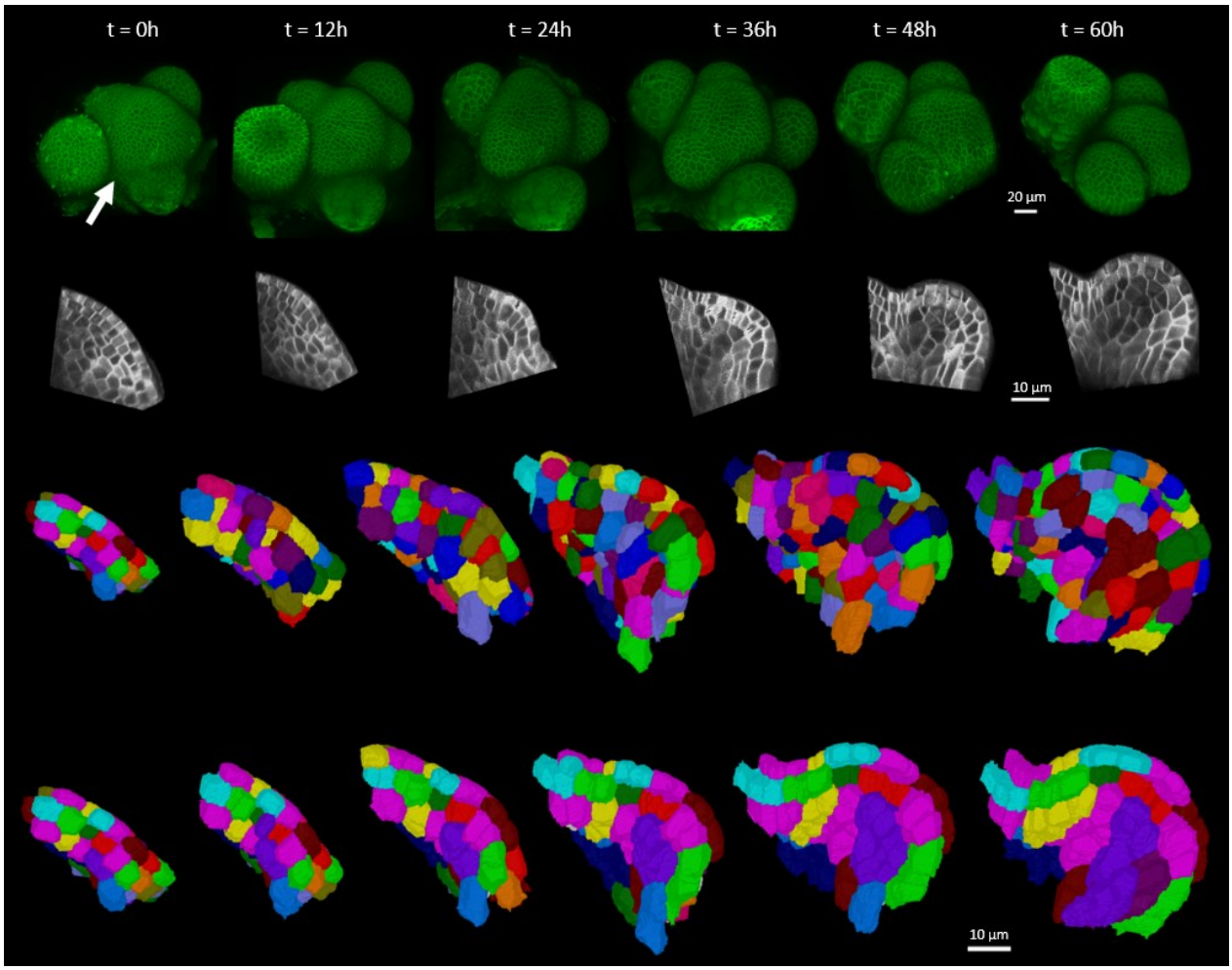

Figure 15: From raw confocal data to 3D lineage tracking, flower 1 sample*. First row: Confocal images on a flower SAM taken at 12 hours interval. Arrow points the targeted flower primordia. Second row: Longitudinal cross-sections of the targeted flower primordia from the above series. Only half of the primordium is shown. Gray coloring is used to emphasize layer delimitation. Third and last rows: Cross-sections of 3D meshes obtained from the above series. In the third row, we see the independent segmentation from individual confocal stack. In the last row, we see how parenting between timepoints allow to follow cell lineage over time.*

3) Comparison of cell dynamics between leaf and flower during primordia initiation

In this section, I present my preliminary results on the comparison of cell dynamics between leaf and flower during early initiation. I describe in detail two representative series, one from a reproductive (called "flower 1") and one from a vegetative meristem (called "leaf 1") (Figure 16; results for additional samples are described in Figures S1 and S2). For both organs, I isolated a bulge at a very early and seemingly comparable stage of development (i.e. incipient primordia stage). The series were representative of the morphology and time evolution observed in other time-lapse series (Figures S1 and S2). All the cross sections presented are longitudinal sections of the organs.

Cell size distribution: regular shapes arise despite local variability in cell sizes

In both flowers and leaves, cells were small and relatively homogeneous in size at the beginning of the developmental series before any bulge was visible (t = 0h, Figures 16, S1 and S2). Cells tended to get bigger as organ development unfolded. In the flower samples, this increase in size was especially noticeable in the internal layers on the abaxial side (t = 48h and 60h, Figure 16; t = 36-48h, Figure S1 A; t = 72-84h, Figure S1 B). In leaves, cells increased in size in all layers as the organ developed. Importantly, cell sizes were very variable between neighbors in both leaves and flowers. No obvious spatial gradient of cell sizes (gradual, smooth increase or decrease in cell size) could be observed within the organ.

Cell divisions do not follow a clear spatial pattern during organ development

In both leaves and flowers, cell divisions occurred in external as well as internal layers with no discernable motif (Figures 16, S1 and S2). As for cell size, no clear spatial pattern of cell division could be observed in any of the series analysed (Figures 16, S1 and S2). In the leaf primordium, the burst of growth observed from the start of the experiment until approximatively 48 hours matches with a burst of division (Leaf 1, Figure 16).

Spatial patterns of cell expansion are associated with organ development

For the flower primordia, I observed a dynamic spatio-temporal distribution of growth. Again, we define growth as the ratio of the total volume (or surface) of a cell progeny over the initial volume of the cell, $\frac{Volume\ of\ cell\ A\ at\ T_{final}}{Volume\ of\ cell\ A\ at\ T_{initial}}$. Growth depends on the time interval (T) being considered. The volume of the cell at T_{final} does not depend on division. Growth was first strong across layers, especially on the abaxial side (t=24h, Figure 16). Toward the end of the observation period, growth gets more homogenous (t=48-

60h, Figure 16). Similar observations were made for the other flower samples (Figure S2, flower 2 and 3). In the leaf primordia, I noticed from the beginning a strong burst on the abaxial side, which attenuated around the latest observed timepoints (Figure 16; Figure S2).

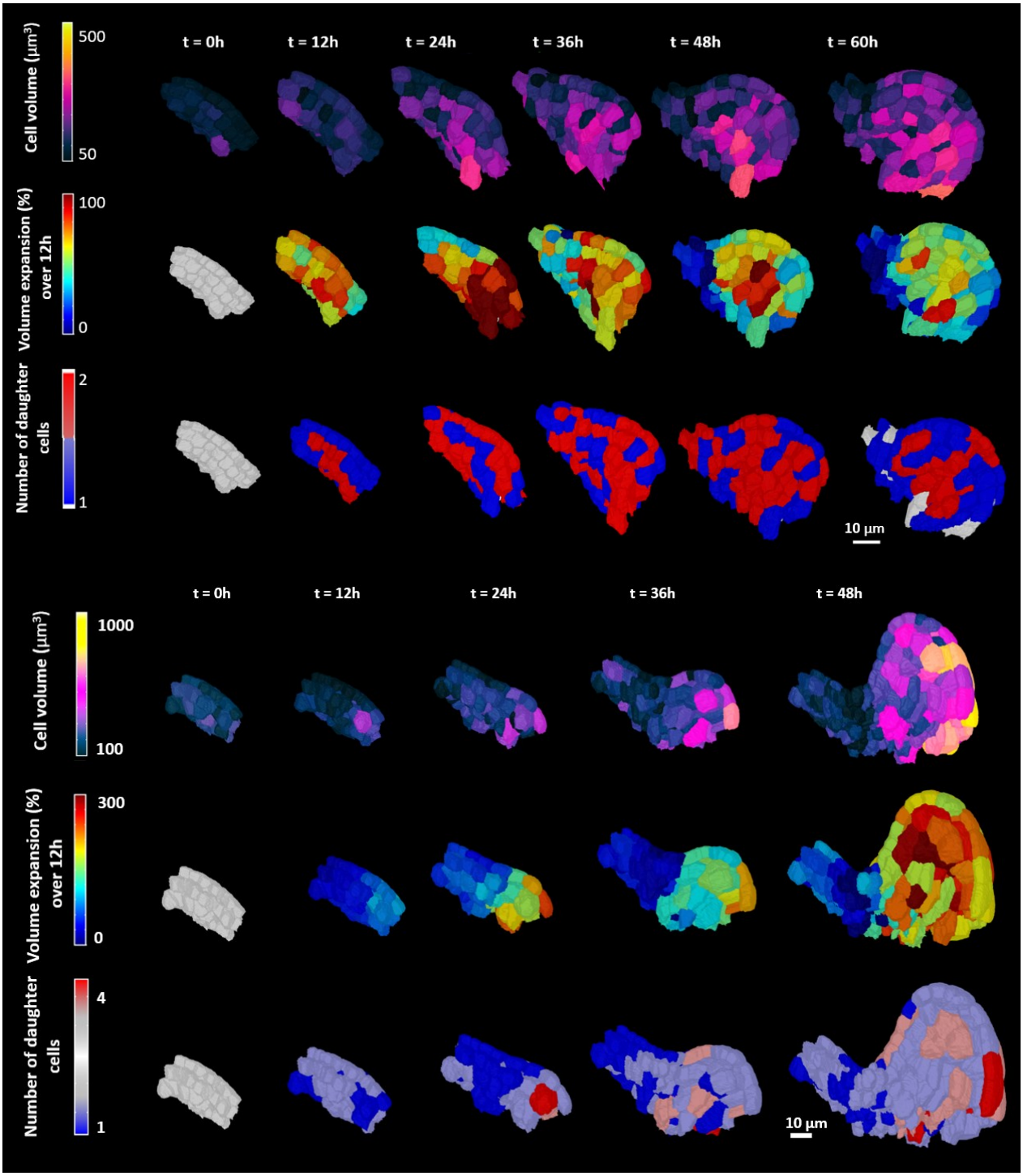

Figure 16: Cell dynamics in flower 1 and leaf 1 primordia. *Longitudinal cross-section view of all analyzed 3D stacks of a reproductive (top) and a vegetative SAM series. Cell volume information were obtained right after 3D segmentation. Cell growth and proliferation information were obtained after parenting all the series. (Top row: cell volume heatmap; middle row: growth heatmap; last row: division heatmap).*

The distribution of growth and cell division: cell expansion is the first sign of organ outgrowth

To further investigate the relationship between cell growth and division, I assessed how growth variation and cell division variation impact one another (Figure 17). For both leaf and flower data, the results suggest that fast growing cells are more prone to have divided at the next observation point (Figure 17, A and C). On the other hand, cells that have divided at one timepoint do not show a significant change in growth at the next timepoint compared to the non-dividing cells (Figure 17, B and D). While we still need to confirm this trend by studying other samples, these results suggest a tendency for fast-growing cells to divide more readily that slowly growing cells. In that regard, as shown by comparing cell growth and division distributions (Figure 16), I conclude that cell division appears to accommodate growth. Therefore, I focused on growth in the next experiments.

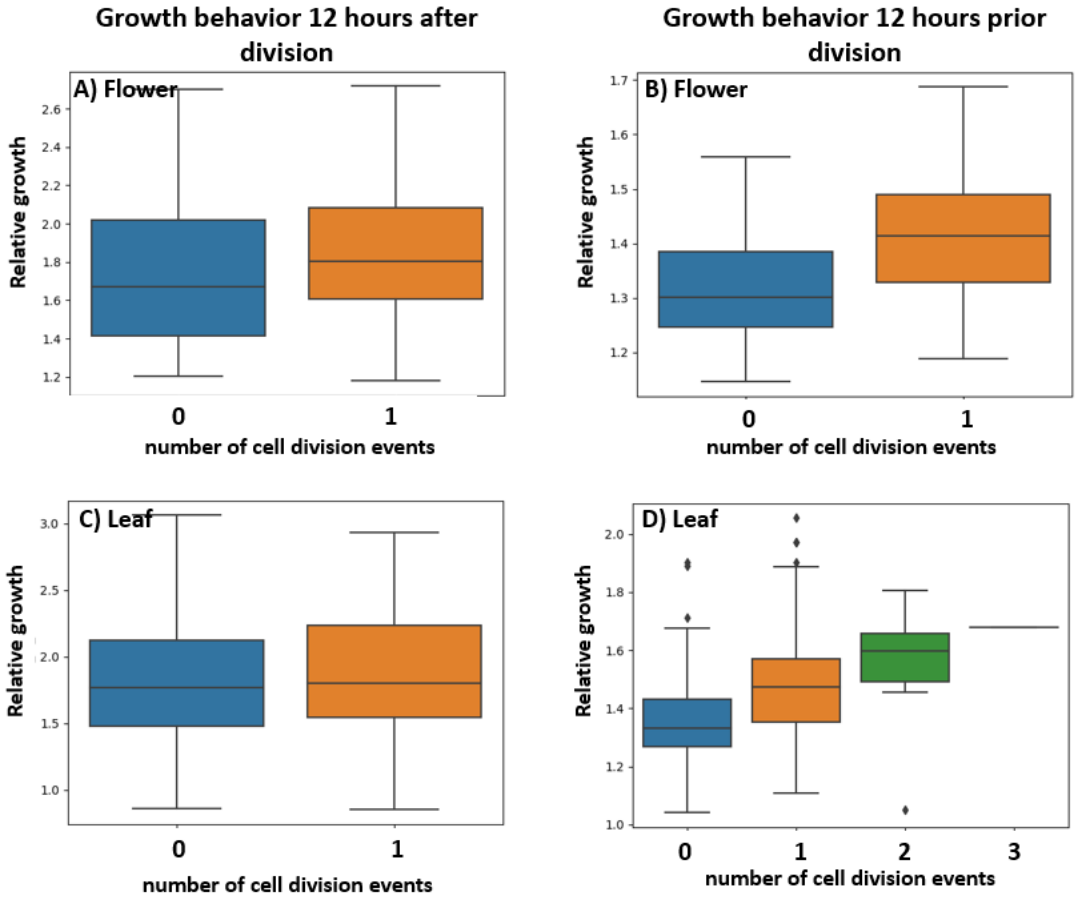

Figure 17: Growth and cell division correlation study. *Impact of cell division on cell growth or cell growth on cell division in flower 1 (A and B) and a leaf 1 (C and D). Cell population for flower: N = 455, for leaf: N = 432. Growth was observed at t=12h in A and C, and at t=24h in B and D. The number of cell divisions was observed at t= 12h in B and D, and at t=24h in A and C.*

4) Which role does each tissue layer play during organ initiation?

Layer contribution to primordia growth

To estimate cell dynamics by layer, I started by isolating complete cell lineages (i.e. from start to end of the time-lapse). Cells at the first timepoint are considered as founder cells of each primordium. A clone is a group of cells derived from the same mother cell (i.e. a founder cell). I followed the growth of those clones in their respective layer (Clones volumes, Figure 18). A clone volume is defined as the combined volume of all the cells in a particular clone. Clone expansion is defined as the growth of an individual founder cell over time (independently of the number of daughter cells). Since I did not collect the same number of founder cells by layer, to confirm our results were not influenced by this difference, I normalized the distribution (clone expansion relative to mother cell volumes, Figure 18). I found that for flower primordia, the clones isolated from the L3 were growing significantly bigger compared to the ones in other layers. Clone expansion is comparable in L1 and L2 (Figures 18 and S1, flower 2 and 3).

For the leaf 1 primordium, growth was dominant in the L2, resulting in an important thickening of the layer (Figures 16 and 18). For the leaf 2 primordium, growth was predominant in the L3 (Figure S3). I have yet to analyse subsequent timepoints of this series. However, raw confocal cross section view of leaf 2 shown a similar cell arrangement as leaf 1 (Figure 3). Thus, I expect similar results.

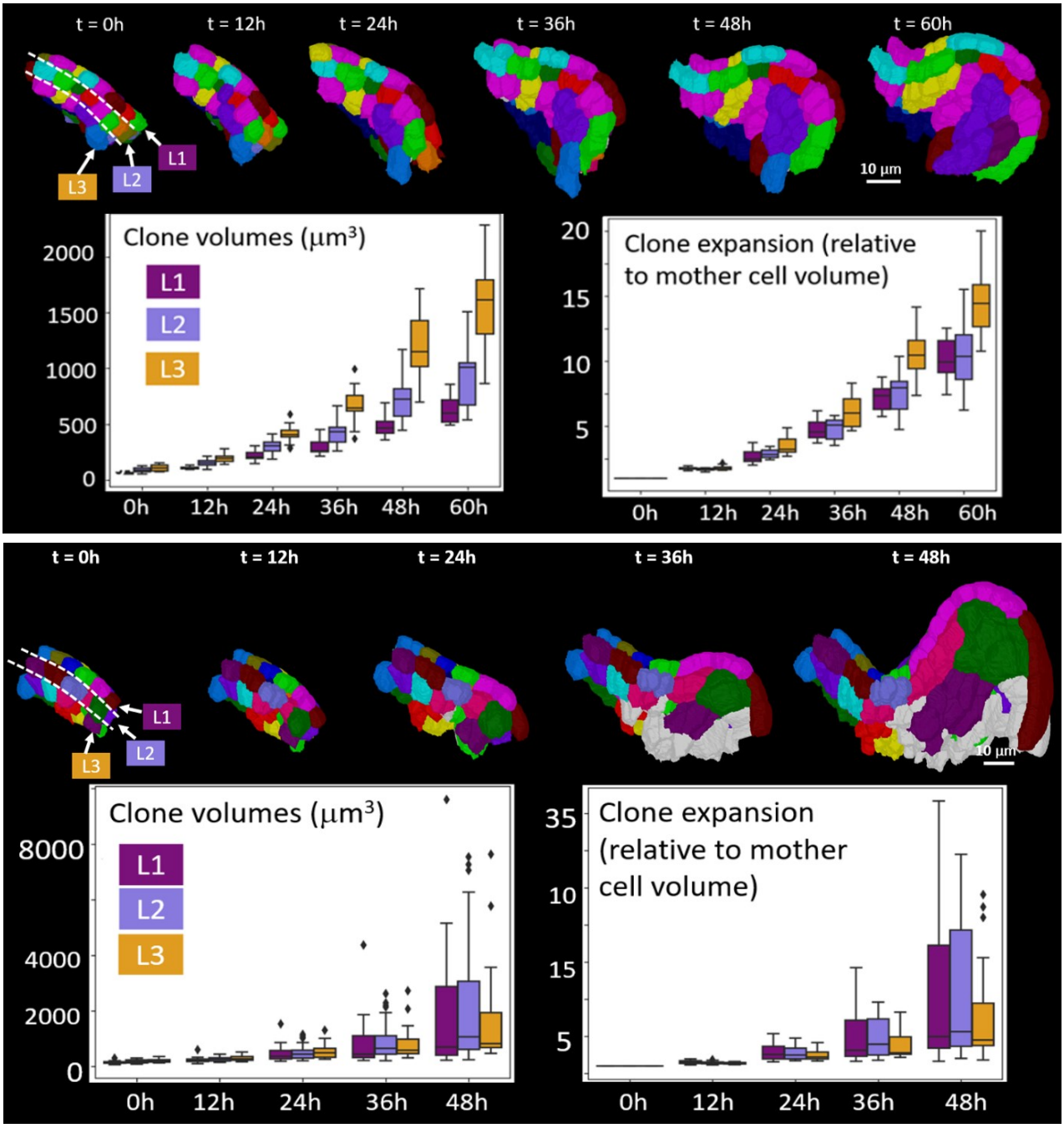

Figure 18: Clonal analysis and statistics for flower (top) and leaf primordia. *A clone is a group of cells derived from the same mother cell (i.e. a founder cell). A clone volume is defined as the combined volume of all the cells in a particular clone. Clone expansion is defined as the growth of an individual founder cell over time (independently of the number of daughter cells). First row: Cross section of flower primordium 3D meshes. Third row: Cross section of flower primordium 3D meshes. Second and fourth row: clone volume, growth and division distributions. For both series, only the clones belonging exclusively to the primordia (not the PZ nor boundary cells) are used in the statistical analysis.*

Discussion

The Method pipeline

The semi-automatized 3D analysis pipeline I develop has allowed to create, for the first time, a spatio-temporal map of flower and leaf primordia cell developmental dynamics. As opposed to other methods (Boudon et al. 2015; Montenegro-Johnson et al. 2019), here I focus on one primordium at the time, limiting 3D segmentation errors. This method is currently used in our lab by other members to answer other biological questions. Compared to previous studies (Grandjean et al. 2004a; Reddy 2004), my methodology allows to retrace complete cell lineage in all meristem layers. Additionally, no other study published so far has described the very first stages of the leaf primordia development in 3D.

Abaxial-adaxial polarity

In leaves and sepal primordia, it was previously shown that growth rates are much higher in the abaxial side compared to the adaxial one, not only in the epidermal, but also in the inner layers (Barbier de Reuille, 2015; McKim, 2017). The high growth rate observed at very early stage of primordia development suggests that abaxial adaxial polarity required for organ outgrowth is established at very earlier stages in all layers. However, for flower primordia, the leaf-like behavior that initially creates the bract is suppressed early at the abaxial side (Figure 19). My results suggest that this spatio-temporal, dynamic repartition of growth in the flower primordia is ultimately responsible for the overall organ shape and its isotropic growth.

In flowers, the strong initial burst of growth coincided with the bract initiation. The later homogeneity in growth distribution could explain the characteristic round shape of the initiating *Arabidopsis* flower. The initial phase of flower primordia outgrowth starts with the bract outgrowth on the abaxial side of the bulge, where growth is the fastest (Figure 16). Combined with the lesser growth observed on the adaxial side, the bract emerges and appears to push outward from the SAM (Figure 19, 24h white arrow). Later on, I observed that growth became weaker at the bract presumably due to molecular changes in the growing organ (Karim et al. 2009). At the same time, the larger cells from the corpus (L3 and subsequent layers) grow bigger due to an important burst of growth, possibly caused by pre-vascularisation and auxin flow (Bayer et al. 2009). As a result, the emerging flower *swells*, like a balloon from the inside. As for the L1 and L2, they seem to mostly accommodate for the growth of the L3 layer and overall bulge. This specific distribution of growth causes the overall round shape characteristic of the flower primordia.

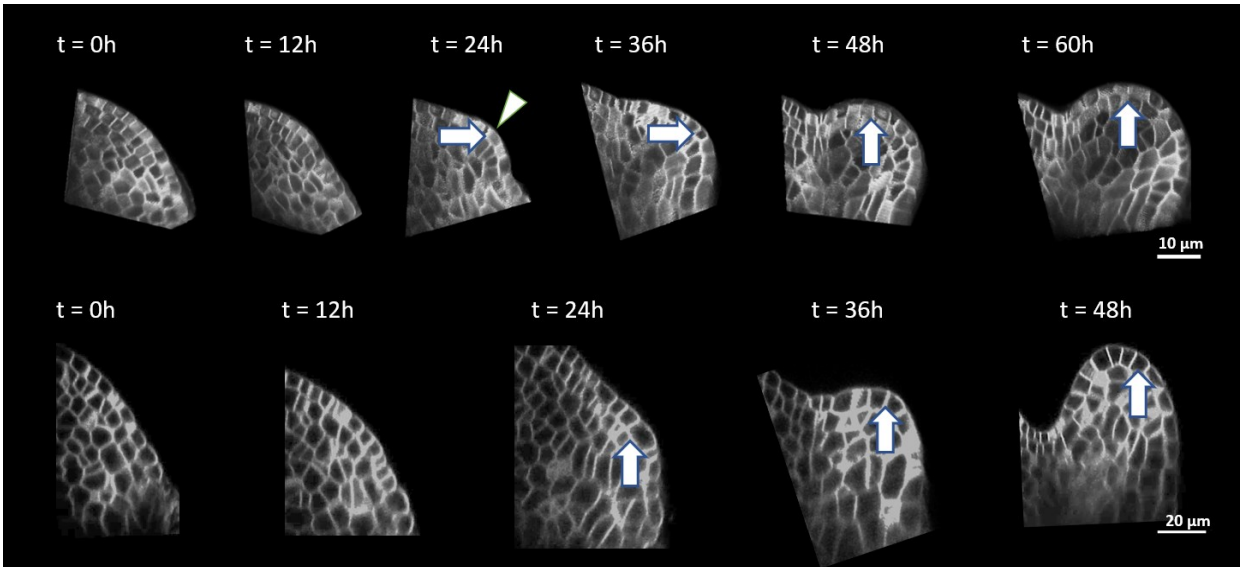

Figure 19: Morphological changes during flower and leaf primordia initiation. *Cross-section view of confocal stacks for the first timepoints of flower 1 and leaf 5 primordia. From my preliminary data, I propose a possible scenario to explain the difference of development between the two organ types. For the flower primordia (top row), a first burst of growth in the abaxial side initiates a bract (arrow). Later (After 48 hours), the change in growth pattern seemingly abolishes the bract development. For the leaf primordia (bottom row), the burst of growth on the abaxial side is not redistributed later, as in the flower primordia. This burst amounts for the asymmetrical cell distribution early in development. This asymmetry in cell size (bigger in abaxial side, smaller in adaxial side) could explain the leaf primordia orientation and early elongated shape later. Leaf 5 had a considerably slower growth and was ignored in the rest of the paper.*

On the other hand, in the leaf primordia, the strong initial burst of growth on the abaxial side could be what causes the initial bending inwards of the leaf, as the cells on the abaxial remain bigger, pushing up then inwards the primordia (Figures 16 and Figure 19). This asymmetrical distribution of growth in the leaf was previously described (Vaughan 1955) and corresponds to the initial tendency of rosette leaves to grow first up, then towards the meristem center, as if to protect it (Vaughan 1955). As discussed by Vaughan previously, I observed that most of the leaf volume is made of the inner layers, especially the L2 which is the main contributing layer forming the leaf primordia.

Take-home message

This study presents a method to analyse cell dynamics in four dimensions. For the first time, the description of the first stages of initiation of not only flower, but also leaf primordia, is presented. By observing additional samples at multiple stages of development, it will finally be possible to draw a clearer picture of plant organ initiation. In the future, this method will be applied to study other organ parts and answer various biological questions.

Supplementary Figures

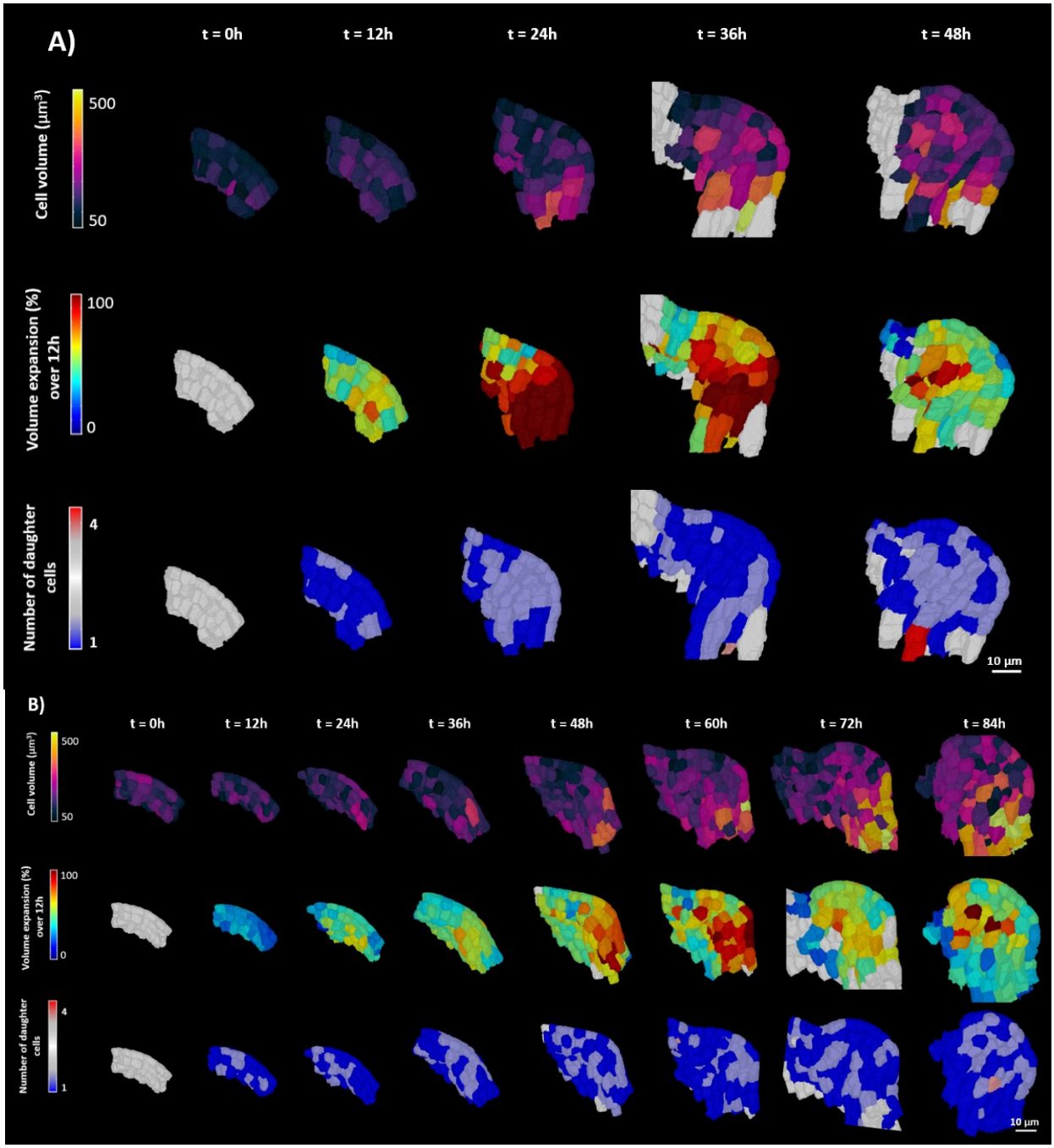

Figure S1: Cell dynamics in flower 2 (A) and flower 3 (B). *Cross-section view of the analyzed 3D stacks are shown for each SAM series. Cell volume information were obtained right after 3D segmentation. Cell growth and proliferation information were obtained after parenting all the series. (Top row: cell volume heatmap; middle row: growth heatmap; last row: division heatmap).*

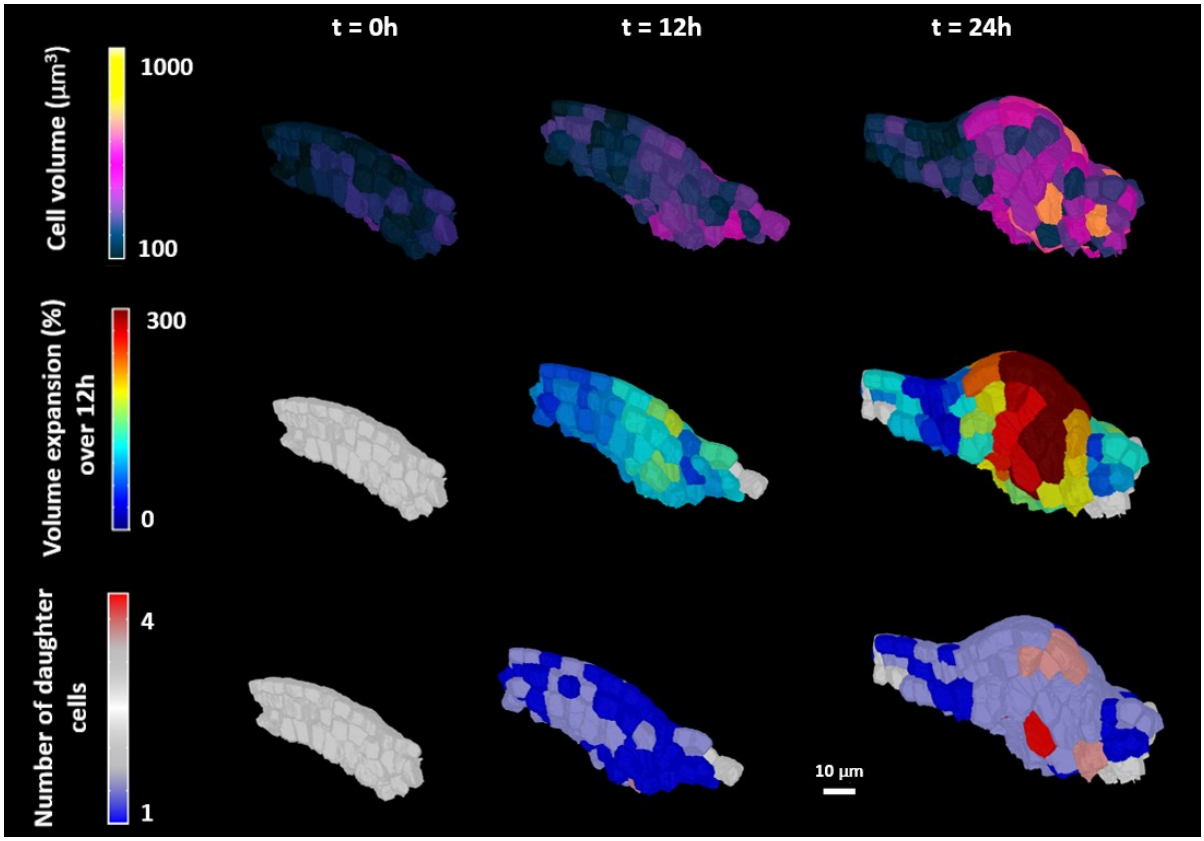

Figure S2: Cell dynamics leaf 2 primordia. *Cross-section view of the analyzed 3D stacks are shown for each SAM series. Cell volume information was obtained right after 3D segmentation. Cell growth and proliferation information were obtained after parenting all the series. (Top row: cell volume heatmap; middle row: growth heatmap; last row: division heatmap).*

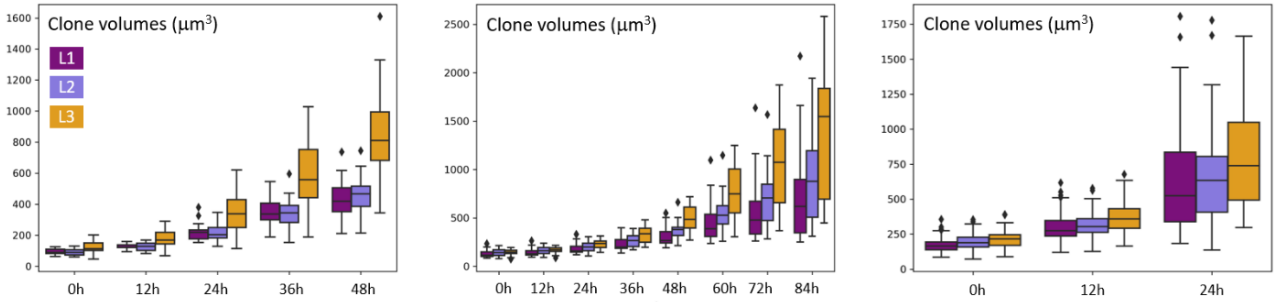

Figure S3: Distribution of clone volumes by layer for flower 2 and 3 primordia (left and middle) and leaf 2 (right) primordia.

Script	Input	Output	Description and Comments
`Create_3D_Stack.py`	• Confocal stack (.tif file)	• Raw 3D stack • Raw 3D mesh • Label list • Segmentation parameters (.info file)	• 3D segmentation and mesh creation • Resulting stack and mesh might still need correction (over/under segmentation) • Raw 3D mesh is used for layer selection • Can work for any .tif file (trimmed or not, depending on processing power)
`Correct_Oversegmentation.py`	• 3D mesh • Target labels to combine	• Fixed 3D mesh • Fixed 3D stack • Updated label list	• Combines label from over segmented mesh • Can work on any 3D mesh (i.e. raw 3D mesh or individual layer mesh) • Can be used at any time during the entire process
`Make_Stack.py`, `Make_All_Stacks.py`	• Label list • Raw 3D stack	• 3D stack of individual layer(s)	• Create the stack of individual layers • The non-sequential version (i.e. `Make_Stack.py`) can be used after correcting over segmentation or cell attribution
`Make_Final_Stack.py`	• Individual 3D stack of desired layers	• Desired combination of 3D mesh for analysis • Corresponding 3D stack	• Generate the combined stack and mesh for a list of timepoints
`Correct_Cell_Attribution.py`	• 3D mesh with excess/missing cells • Corresponding complementary mesh	• Fixed 3D meshs • Updated label lists	• Re-assign cells between two adjacent layers. From the two layer meshes, the script returns the corrected versions of the meshes and cell label list.
`Combine_*.py`	• information .csv files from different layers at the same timepoint	• Combined .csv file information for a given timepoint	• Combine information (parenting, layer position, growth, ect,…) into a single file for a given timepoint
`BackZoning.py`, `ForwardZoning.py`	• Parenting information .csv files • Clone, layer, or zone information .csv file at a timepoint Tn	• Clone, layer or zone information .csv at Tn-1 and earlier timepoints (`BackZoning.py`) or at Tn+1 and successive timepoints (`ForwardZoning.py`)	• Establish cell lineage between timepoints and track back or forward zone information along a series of timepoints.

Table 1: Table of the main Python scripts (description and usage) of the pipeline.

Sample name in this paper	Sample original name
Flower 1	2020128_102_PM_YFP_repSAM_22
Flower 2	2020128_102_PM_YFP_repSAM_01
Flower 3	20200717_102_PM_YFP_rep_SAM_02
Flower 4	200713_veg_SAM_18 (Flower 1)
Leaf 1	20200724_102_PM_YFP_veg_SAM_03
Leaf 2	20200724_102_PM_YFP_veg_SAM_06
Leaf 3	20200724_102_PM_YFP_veg_SAM_05
Leaf 4	20200724_102_PM_YFP_veg_SAM_08

Table 2: List of the samples described and their equivalent names in this paper.

Glossaire

Anticlinal divisions: Cells have a division plan perpendicular to the organ surface. Cells from an anticlinal division will remain in the same tissue layer.

Apex: meristem with adjacent organ primordia that are deliminated from the meristem by nascent or distinct boundaries (= slightly negative curvature value and concave surface). The apex delimitation is formed of the meristem border and clearly delimited (= deep negative curvature value) primordia.

Bract: Leaf-like organ formed at a flower bud. In Arabidopsis, the bract is abolished early in development (Long and Barton, 2000; Dumais and Kwiatkowska, 2006).

Cell dynamics: here, cell dynamics is a term that englobes overall cell behaviors in terms of size, growth or proliferation.

Clone: group of descendants of a cell at later timepoints. Here, a clonal sector represents the portion of a SAM emerging from a single cell.

Growth: Here, we define growth as the ratio of the total volume (or surface) of a cell progeny over the initial volume of the cell, $\frac{Volume\ of\ cell\ A\ at\ T_{final}}{Volume\ of\ cell\ A\ at\ T_{initial}}$. Growth depends on the time interval (T) being considered. The volume of the cell at T_{final} does not depend on division: if a division as taken place between $T_{initial}$ and T_{final}, both daughter cells volume are considered in the final volume.

Inflorescence: clusters of flower meristems (apex with more developed flowers not visible in a stack or bigger developing flower meristems from the stack).

Meristem: cluster of cells (or stem cell niche). In the SAM, zone in which there is no (nascent or clean) boundary yet between the PZ and the incipient or adjacent primordia.

Mesh: In surface segmentation, a mesh describes the approximated molding of an object. In 3D segmentation, the corresponding mesh is in fact the combined moldings of each cell (Barbier de Reuille, 2015). In this project, meshes are produced in MorphographX™ to store information about cells, such as their size (or volume, in 3D), position within the sample, and so on.

Parenting: in MorphographX™, parenting is the operation of assigning a parent label from a given timepoint to all progeny cell at a later timepoint. Parenting is necessary to establish cell lineage in a series.

Periclinal divisions: Cells have a division plane parallel to the organ surface. Daughter cells from such divisions might end up in a different tissue layer.

Phyllotaxis: regular arrangement of leaves or flowers at a plant stem. Most studied example of pattern formation and organogenesis.

Plastochron: time interval between two successive organ initiation events.

Primordia: group of cells from which organs are initiated.

Segmentation: in MorphographX™, segmentation describes all processing steps from stack mask (mold) conversion, mesh creation and signal projection.

Staging: attribution of a precise developmental stage to a group of cells.

References

Barbier de Reuille, Pierre, Anne-Lise Routier-Kierzkowska, Daniel Kierzkowski, George W. Bassel, Trudi Schüpbach, Gerardo Tauriello, Namrata Bajpai, et al. 2015. "MorphoGraphX: A Platform for Quantifying Morphogenesis in 4D." *ELife* 4: 1–20. https://doi.org/10.7554/eLife.05864.

Bayer, Emmanuelle M, Richard S Smith, Therese Mandel, Naomi Nakayama, Michael Sauer, Przemyslaw Prusinkiewicz, and Cris Kuhlemeier. 2009. "Integration of Transport-Based Models for Phyllotaxis and Midvein Formation." *Genes and Development* 23 (3): 373–84. https://doi.org/10.1101/gad.497009.

Benková, Eva, Marta Michniewicz, Michael Sauer, Thomas Teichmann, Daniela Seifertová, Gerd Jü Rgens, and Jiří Friml. 2003. "Local, Efflux-Dependent Auxin Gradients as a Common Module for Plant Organ Formation Growing Shoots or Roots Bearing a Secondary Meristem at the Tip. Aerial Organs Such as Leaves and Secondary Shoots, Including Flowers, Originate from Primordia On." *Cell*. Vol. 115.

Boudon, Frédéric, Jérôme Chopard, Olivier Ali, Benjamin Gilles, Olivier Hamant, Arezki Boudaoud, Jan Traas, and Christophe Godin. 2015. "A Computational Framework for 3D Mechanical Modeling of Plant Morphogenesis with Cellular Resolution." *PLoS Computational Biology* 11 (1): 1003950. https://doi.org/10.1371/journal.pcbi.1003950.

Carraro, Nicola, Alexis Peaucelle, Patrick Laufs, and Jan Traas. 2006. "Cell Differentiation and Organ Initiation at the Shoot Apical Meristem." *Plant Molecular Biology*. https://doi.org/10.1007/s11103-005-2761-6.

Grandjean, Olivier, Teva Vernoux, Patrick Laufs, Katia Belcram, Yuki Mizukami, and Jan Traas. 2004a. "The Plant Cell In Vivo Analysis of Cell Division, Cell Growth, and Differentiation at the Shoot Apical Meristem in Arabidopsis." *The Plant Cell* 16: 74–87. https://doi.org/10.1105/tpc.017962.

———. 2004b. "In Vivo Analysis of Cell Division, Cell Growth, and Differentiation at the Shoot Apical Meristem in Arabidopsis." *The Plant Cell* 16 (1): 74–87. https://doi.org/10.1105/tpc.017962.

Jones, Angharad, Manuel Forero-Vargas, Simon P. Withers, Richard S. Smith, Jan Traas, Walter Dewitte, and James A. H. Murray. 2017. "Cell-Size Dependent Progression of the Cell Cycle Creates Homeostasis and Flexibility of Plant Cell Size." *Nature Communications* 8 (April): 15060.

https://doi.org/10.1038/ncomms15060.

Karim, Md Rezaul, Atsuko Hirota, Dorota Kwiatkowska, Masao Tasaka, and Mitsuhiro Aida. 2009. “A Role for Arabidopsis PUCHI in Floral Meristem Identity and Bract Suppression.” *Plant Cell* 21 (5): 1360–72. https://doi.org/10.1105/tpc.109.067025.

Kierzkowski, Daniel, Naomi Nakayama, Anne-Lise Routier-Kierzkowska, Alain Weber, Emmanuelle Bayer, Martine Schorderet, Didier Reinhardt, Cris Kuhlemeier, and Richard S Smith. 2012. “Elastic Domains Regulate Growth and Organogenesis in the Plant Shoot Apical Meristem.” *Science* 335 (6072): 1096–99. https://doi.org/10.1126/science.1213100.

Kwiatkowska, D. 2004a. “Surface Growth at the Reproductive Shoot Apex of Arabidopsis Thaliana Pin-Formed 1 and Wild Type.” *Journal of Experimental Botany* 55 (399): 1021–32. https://doi.org/10.1093/jxb/erh109.

———. 2004b. “Surface Growth at the Reproductive Shoot Apex of Arabidopsis Thaliana Pin-Formed 1 and Wild Type.” *Journal of Experimental Botany* 55 (399): 1021–32. https://doi.org/10.1093/jxb/erh109.

Kwiatkowska, Dorota, and Jacques Dumais. 2003. “Growth and Morphogenesis at the Vegetative Shoot Apex of Anagallis Arvensis L.” *Journal of Experimental Botany* 54 (387): 1585–95. https://doi.org/10.1093/jxb/erg166.

Kwiatkowska, Dorota, and Anne-Lise Routier-Kierzkowska. 2009. “Morphogenesis at the Inflorescence Shoot Apex of Anagallis Arvensis: Surface Geometry and Growth in Comparison with the Vegetative Shoot.” *Journal of Experimental Botany* 60 (12): 3407–18. https://doi.org/10.1093/jxb/erp176.

Long, Jeff, and M Kathryn Barton. 2000. “Initiation of Axillary and Floral Meristems in Arabidopsis.” https://doi.org/10.1006/dbio.1999.9572.

Montenegro-Johnson, Thomas, Soeren Strauss, Matthew D.B. Jackson, Liam Walker, Richard S. Smith, and George W. Bassel. 2019. “3DCellAtlas Meristem: A Tool for the Global Cellular Annotation of Shoot Apical Meristems.” *Plant Methods* 15 (1): 33. https://doi.org/10.1186/s13007-019-0413-0.

Parcy, François, Ove Nilsson, Maximilian A. Busch, Ilha Lee, and Detlef Weigel. 1998. “A Genetic Framework for Floral Patterning.” *Nature* 395 (6702): 561–66. https://doi.org/10.1038/26903.

Reddy, G. V. 2004. “Real-Time Lineage Analysis Reveals Oriented Cell Divisions Associated with Morphogenesis at the Shoot Apex of Arabidopsis Thaliana.” *Development*. https://doi.org/10.1242/dev.01261.

Reddy, G. V., Marcus G. Heisler, David W. Ehrhardt, and Elliot M. Meyerowitz. 2004. “Real-Time Lineage Analysis Reveals Oriented Cell Divisions Associated with Morphogenesis at the Shoot Apex of Arabidopsis Thaliana.” *Development* 131: 4225–37. https://doi.org/10.1242/dev.01261.

Smith, R. S., S. Guyomarc’h, T. Mandel, D. Reinhardt, C. Kuhlemeier, and P. Prusinkiewicz. 2006. “A Plausible Model of Phyllotaxis.” *Proceedings of the National Academy of Sciences* 103 (5): 1301–6. https://doi.org/10.1073/pnas.0510457103.

Soyars, Cara L., Sean R. James, and Zachary L. Nimchuk. 2016. “Ready, Aim, Shoot: Stem Cell Regulation of the Shoot Apical Meristem.” *Current Opinion in Plant Biology*. Elsevier Ltd. https://doi.org/10.1016/j.pbi.2015.12.002.

Steeves, Taylor, and Ian M Sussex. 1989. *Patterns in Plant Developpement*. 2nd ed. Cambridge University Press.

Tian, Caihuan, Ying Wang, Haopeng Yu, Jun He, Jin Wang, Bihai Shi, Qingwei Du, Nicholas J Provart, Elliot M Meyerowitz, and Yuling Jiao. 2019. “A Gene Expression Map of Shoot Domains Reveals Regulatory Mechanisms.” *Nature Communications* 10 (1). https://doi.org/10.1038/s41467-018-08083-z.

Vaughan, J. G. 1955. “The Morphology and Growth of the Vegetative and Reproductive Apices of Arabidopsis Thaliana (L.) Heynh., Capsella Bursa-pastoris (L.) Medic. and Anagallis Arvensis L.” *Journal of the Linnean Society of London, Botany* 55 (359): 279–301. https://doi.org/10.1111/j.1095-8339.1955.tb00014.x.

Willis, Lisa, Yassin Refahi, Raymond Wightman, Benoit Landrein, José Teles, Kerwyn Casey Huang, Elliot M Meyerowitz, and Henrik Jönsson. 2016. “Cell Size and Growth Regulation in the Arabidopsis Thaliana Apical Stem Cell Niche.” *Proceedings of the National Academy of Sciences of the United States of America* 113 (51): E8238–46. https://doi.org/10.1073/pnas.1616768113.

Yang, Weibing, Christoph Schuster, Cherie T T. Beahan, Varodom Charoensawan, Alexis Peaucelle, Antony Bacic, Monika S S. Doblin, Raymond Wightman, and Elliot M M. Meyerowitz. 2016. “Regulation of Meristem Morphogenesis by Cell Wall Synthases in Arabidopsis.” *Current Biology* 26

(11): 1404–15. https://doi.org/10.1016/j.cub.2016.04.026.

Journal of Experimental Botany, Vol. 70, No. 14 pp. 3573–3585, 2019
doi:10.1093/jxb/erz205 Advance Access Publication 30 April, 2019

REVIEW PAPER

Growth and biomechanics of shoot organs

Emilie Echevin[1], Constance Le Gloanec[1], Nikolina Skowrońska[2], Anne-Lise Routier-Kierzkowska[1], Agata Burian[2] and Daniel Kierzkowski[1,*]

[1] Institut de Recherche en Biologie Végétale, Department of Biological Sciences, University of Montreal, 4101 Sherbrooke Est, Montréal H1X 2B2, QC, Canada
[2] Department of Biophysics and Morphogenesis of Plants, University of Silesia, Jagiellońska 28, 40-032 Katowice, Poland

*Correspondondence: daniel.kierzkowski@umontreal.ca

Received 2 February 2019; Editorial decision 17 April 2019; Accepted 17 April 2019

Editor: Anja Geitmann, McGill University, Canada

Abstract

Plant organs arise through complex interactions between biological and physical factors that control morphogenesis. While there has been tremendous progress in the understanding of the genetics behind development, we know much less about how mechanical forces control growth in plants. In recent years, new multidisciplinary research combining genetics, live-imaging, physics, and computational modeling has begun to fill this gap by revealing the crucial role of biomechanics in the establishment of plant organs. In this review, we provide an overview of our current understanding of growth during initiation, patterning, and expansion of shoot lateral organs. We discuss how growth is controlled by physical forces, and how mechanical stresses generated during growth can control morphogenesis at the level of both cells and tissues. Understanding the mechanical basis of growth and morphogenesis in plants is in its early days, and many puzzling facts are yet to be deciphered.

Keywords: Cell wall, flowers, growth, leaves, mechanical feedback, mechanical stress, morphogenesis, organogenesis, shoot lateral organs, turgor pressure.

Introduction

The development of multicellular organisms generates an astonishing variety of biological forms. In plants, organ shapes and sizes emerge from the precise coordination of cell growth, cell division, patterning, and differentiation (Sablowski, 2015). As plant cells are glued together via their stiff cell walls, these developmental processes occur within mechanically connected tissues. Such physical constraints play a critical role during plant development and act as an instructive signal to control organogenesis (Hamant, 2017). While the genetic basis of morphogenesis has been extensively studied (Ingram and Mähönen, 2018), we are still far from understanding how biomechanics interacts with genetic factors and modulates organ growth.

At the cellular level, growth occurs as the cell wall yields under internal turgor pressure (Cosgrove, 2018). Cell growth, therefore, depends on the mechanical properties of cell walls, which are determined by their composition and structure. According to the current model, the cell wall is a network of cellulose microfibrils linked by hemicellulose and embedded in a pectin matrix (Cosgrove, 2000). Cellulose microfibrils are the main load-bearing element of the wall and their orientation constrains the directionality (anisotropy) of cell growth (Ehrhardt and Shaw, 2006). Wall-remodeling enzymes, acting on both hemicellulose and pectin, modulate the growth rate by stiffening or loosening the wall (Braybrook and Jönsson, 2016; Cosgrove, 2018). Heterogenous mechanical

and chemical properties of cell walls can also contribute to anisotropic growth (Peaucelle *et al.*, 2015; Majda *et al.*, 2017; Bou Daher *et al.*, 2018). Additionally, cell geometry (shape and size) is a pivotal factor in controlling cellular growth via its effect on tensile stresses (reviewed in Kierzkowski and Routier-Kierzkowska, 2019).

While biomechanics at the cell level is easier to capture, understanding mechanics at the organ level is still challenging (Box 1). Mechanical properties of cells and tissues can directly control the expansion and shape of the developing organ (Coen *et al.*, 2004). On the other hand, variation in the rate and direction of growth between neighboring cells and tissues creates mechanical conflicts (Rebocho *et al.*, 2017). Such a passive mechanism creates residual stresses that may feed back on expansion.

A multidisciplinary approach that integrates biology, physics, and computer science is needed to assess the exact contribution of physical forces in plant morphogenesis. Recent methodological improvements in time-lapse imaging (Hervieux *et al.*, 2016; Fox *et al.*, 2018; Jackson *et al.*, 2019), mechanical measurements (Kierzkowski *et al.*, 2012; Routier-Kierzkowska *et al.*, 2012; Beauzamy *et al.*, 2015*b*), image analysis (Barbier de Reuille *et al.*, 2015), and computer modeling (Sassi *et al.*, 2014; Bassel and Smith, 2016; Bidhendi and Geitmann, 2018a, b; Sapala *et al.*, 2018) progressively reveal the links between biomechanics and plant development. In this review, we discuss the biomechanics of growth in leaves and flowers, focusing on the stages of organ initiation, patterning, and expansion.

Initiation of lateral organs

Plant shoots produce several types of lateral organs, including: (i) leaves, which are the main photosynthetic organs; and (ii) flowers, which are critical for plant reproduction. Flowers are composed of both non-reproductive (sepals and petals) and reproductive (pistils and carpels) organs. Genetic studies show that leaves can be converted into floral organs and vice versa, suggesting that all lateral organs are likely to have evolved from a leaf-like ancestor (Bowman *et al.*, 1991; Coen and Meyerowitz, 1991; Pelaz *et al.*, 2001).

Leaves and flowers are initiated at the tip of the plant shoot, which contains the shoot apical meristem (SAM) (Steeves and Sussex, 1989). During vegetative development, leaf primordia appear as small protrusions in the peripheral zone of the SAM (Clark, 1997) (Fig. 1). After the transition to flowering, the initiation of a leaf primordium (bract) is followed by a flower primordium, which forms at the boundary between the young leaf and the meristem (Alvarez-Buylla *et al.*, 2010). In most plant species, this leaf primordium will develop into a bract associated with the flower. In other species, including

Box 1. Mechanical stresses at different levels and their assessment

- **Stress at the cellular level**

  The walls of turgid plant cells are stretched due to internal pressure. Tension in the cell wall, also called tensile stress, is proportional to the turgor pressure. However, cell wall tension also depends on cell geometry. For a sphere or cube-shaped cell, at equal pressure, tensile stress will be higher in a large cell than in a small one (Bassel *et al.*, 2014). In cells of more complex shapes, stress depends on local geometry and does not necessarily increase with cell volume (Sapala *et al.*, 2018).

- **Stress at the tissue level**

  Cells are glued to each other within tissues, which constrains the way they can deform under pressure and grow. For example, a cell with stiffer walls would 'pull' on its softer neighbors, changing the stress pattern locally. We call these additional mechanical forces 'residual stresses' or 'tissue stresses', since they can only exist in tissues and add up to the cellular stresses mentioned above.

- **Stress at the organ level**

  Tissue layers are connected to each other within an organ, which limits their deformation and creates additional stresses. For instance, consider an outer tissue layer that would shrink when pressurized and an inner layer that would be much stiffer and would not deform. If the layers are attached to each other, the outer one will pull on the inner one when pressurized, generating tension in the outer layer and compression in the inner layer (Hofhuis *et al.*, 2016). Similarly, isolated tissue layers could have different intrinsic growth rates. Once connected to each other, these differences would cause 'growth-based stresses' within the organ (Baskin and Jensen, 2013).

- **Assessing mechanical stresses**

  Mechanical stresses cannot be measured directly. Mechanical simulations are used to compute stresses at the cellular, tissue or organ levels (reviewed by Routier-Kierzkowska and Runions, 2018). Models rely on several assumptions, which can affect the computed stresses. Microtubule orientation is often used as a proxy for the direction of maximal stress. However, this does not distinguish between cellular-, tissue-, or organ-level stresses nor indicate the magnitude of stresses. Cuts and ablations are used to assess the orientation of stresses at the organ level. Again, this method does not show the amplitude of stresses.

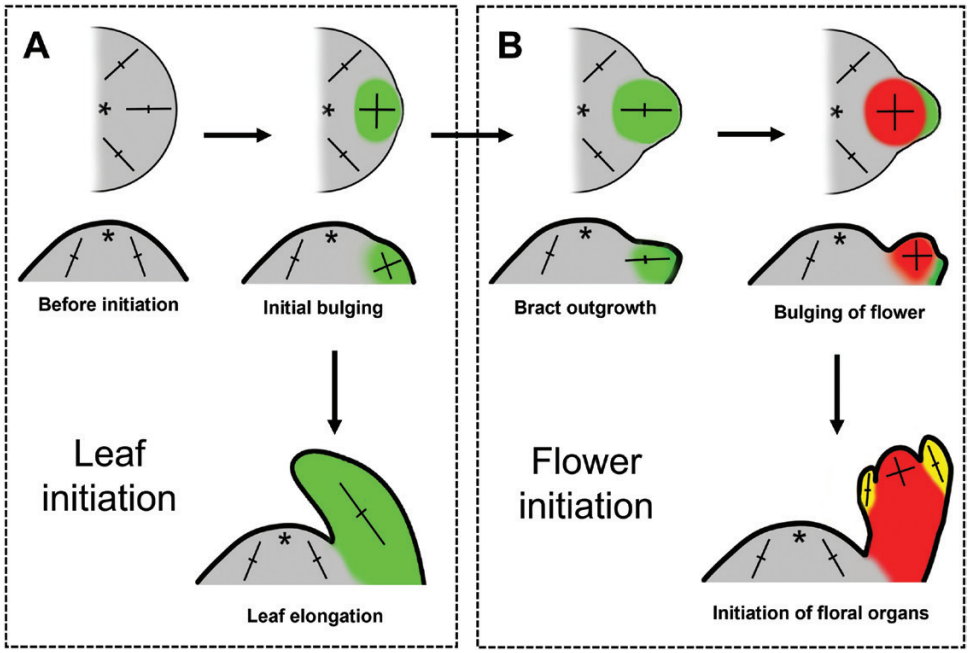

Fig. 1. Morphological events during lateral organ initiation in Arabidopsis. (A) Schematic representation of leaf initiation. At initiation, cells in the SAM peripheral zone expand radially. During leaf bulging (in green), growth is fast and isotropic. This is followed by fast primordium elongation along its proximo-distal axis. (B) Schematic representation of flower initiation. After initial bulging, the bract primordium (in green) expands in the radial direction. Subsequently, fast and isotropic growth occurs at the initiating flower primordium (in red). While the growth rate at the center of the newly formed flower primordium decreases, the sepals (in yellow) are initiated, and expand rapidly along their proximo-distal axis. The upper row represents a top view and bottom rows the side views of the meristems. Only the organ surface is considered. Asterisks indicate the SAM center. Crosses indicate the principal directions of growth.

Arabidopsis, bract development is repressed quickly after its initiation. Nevertheless, the first signs of floral primordium outgrowth in Arabidopsis indicate bract initiation (Long and Barton, 2000; Kwiatkowska, 2006). The flower primordium subsequently develops into the flower meristem, whose activity is determinate, producing a finite number of floral organs arranged in whorls (Smyth *et al.*, 1990).

During organ initiation, cells increase their growth and division rates to form a primordium. Meanwhile, growth decreases in cells directly neighboring the emerging organ, leading to the establishment of boundary zones that separate primordia from each other and from the SAM (Kwiatkowska and Dumais, 2003; Breuil-Broyer *et al.*, 2004; Kwiatkowska, 2004; Kierzkowski *et al.*, 2012; McKim *et al.*, 2017; Monniaux *et al.*, 2018). Growth patterns differ between leaf and flower primordia (Kwiatkowska, 2006; Burian *et al.*, 2016), but are very similar during early growth of leaves and sepals (Hervieux *et al.*, 2016; McKim *et al.*, 2017). During leaf initiation, cell growth rates not only increase but also become more isotropic (equal in all directions) in comparison with the surrounding peripheral zone where cells grow faster in the radial direction (Kwiatkowska and Dumais, 2003*b*; Barbier de Reuille *et al.*, 2015) (Fig. 1A). In leaves and sepals, organ boundaries first appear as regions of slower growth around the primordium (Kwiatkowska, 2006; McKim *et al.*, 2017). After bulging, the leaf or sepal primordium rapidly elongates along its primordium proximo-distal axis, which is reflected in highly anisotropic growth observed at the cellular level (Schiessl *et al.*, 2012; Barbier de Reuille *et al.*, 2015). Sepals and leaves bend toward the meristem since their growth rate is much higher on the abaxial side (Barbier de Reuille *et al.*, 2015; Hervieux *et al.*, 2016; McKim *et al.*, 2017). Flower initiation starts with the formation of a bract primordium, which resembles leaf initiation at early stages. In Arabidopsis, the bract primordium then rapidly elongates in the radial direction (Reddy *et al.*, 2004; Kwiatkowska, 2006; Kwiatkowska and Routier-Kierzkowska, 2009). Finally, the flower primordium bulges at the bract boundary via fast and isotropic growth (Fig. 1B).

Growth patterns during the initiation and outgrowth of internal floral organs are unknown. Even the description of early growth in flowers and leaves is incomplete and mostly based on observations of just a few model species: *Anagalis* and tomato during the vegetative phase, and Arabidopsis and *Anagalis* after the transition to flowering. Additionally, some aspects of flower initiation seem to be different between species (Kwiatkowska, 2006; Kwiatkowska and Routier-Kierzkowska, 2009). We clearly need more growth studies in different species and mutants to fully understand and generalize the events occurring during organ initiation. This gap will be likely filled thanks to the intensive development of live-imaging techniques.

Biomechanical aspects of organ initiation

It is generally accepted that the outer cell layer of the meristem is under tension and the underlying tissues are under compression (Green *et al.*, 1996; Kutschera and Niklas, 2007; Kierzkowski *et al.*, 2012; Beauzamy *et al.*, 2015*b*). However, the biomechanical basis of organ initiation is still debated, and competing conceptual models have been proposed (Fig. 2). Model

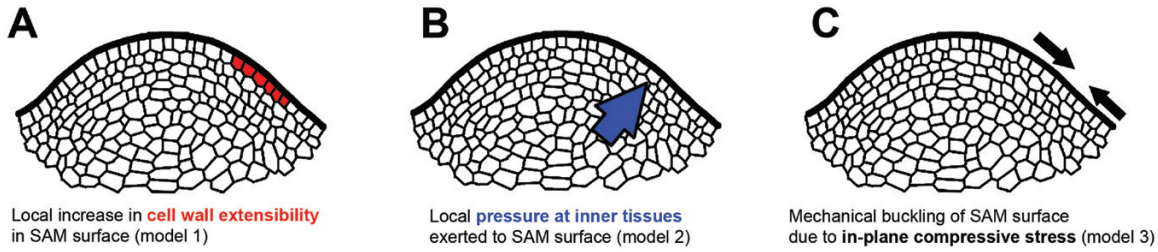

Fig. 2. Current biomechanical models of organ initiation. (A) Local cell wall extensibility increases in the outer layer, which results in a relaxation of the tensile stresses in the outer layers, and subsequent relaxation of the compressive forces in the inner layers (Fleming, 2006). (B) Local growth rate increases in the inner layers positioned directly underneath the future primordium, resulting in a strong local pressure exerted on the external layer (Peaucelle *et al.*, 2011). (C) Radially oriented, in-plane compressive stress resulting from the meristem geometry or from the differential growth of various SAM regions leads to mechanical buckling of the SAM surface (Selker *et al.*, 1992).

1 proposes that organ formation is triggered by a local increase in cell wall extensibility in the outer cell layers (Fleming, 2006; Cosgrove, 2016), leading to the relaxation of tensile and compressive stresses in the outer and inner layers, respectively (Fig. 2A). Model 2 proposes that the inner tissues exert pressure on external layers through the local increase of growth rates in a direction perpendicular to the surface (Selker *et al.*, 1992; Peaucelle *et al.*, 2011) (Fig. 2B). Assuming that the outer layers are not softened, this would lead to an increase in mechanical stresses across layers. Both models assume that mechanical properties change only at the site of initiation. In contrast, model 3 proposes that organ initiation could occur without such local modification. Excessive growth of the outer layer compared with the internal layers would result in building up of compressive stresses within the outer layers. The meristem surface would buckle, releasing stresses and forming bulges which develop into primordia (Fig. 2C) (Green and Selker, 1991; Selker *et al.*, 1992; Dumais and Steele, 2000; Newell and Shipman, 2005).

The plant hormone auxin is the only molecule known to date that is both required and sufficient for organ initiation (Reinhardt *et al.*, 2000, 2003). Local auxin concentration maxima form in the surface layer of incipient primordia by the activity of the PINFORMED1 (PIN1) auxin efflux carrier (Reinhardt *et al.*, 2003; Heisler *et al.*, 2005; Smith *et al.*, 2006; Bayer *et al.*, 2009; Kierzkowski *et al.*, 2013). Local auxin applications restore organogenesis at the SAMs which are unable to form organs (Reinhardt *et al.*, 2003). Auxin affects cell wall mechanics and growth by activating transcriptional and non-transcriptional responses (Edelmann and Kutschera, 1993; Overvoorde *et al.*, 2005; Leyser, 2018), namely stimulation of plasma membrane proton pumps, causing cell wall acidification and loosening (Kutschera and Niklas, 2007; Takahashi *et al.*, 2012). Thus, auxin could be associated with a local increase in cell wall extensibility at the SAM surface according to model 1.

Auxin-induced organ initiation can be mimicked by molecules that affect cell wall mechanics. Expansins, cell wall proteins implicated in cell wall relaxation (McQueen-Mason and Cosgrove, 1995), are up-regulated at the incipient primordia in tomato (Reinhardt *et al.*, 1998). The local application of expansins at the SAM surface induces the initiation of an abnormal leaf-like primordium (Fleming *et al.*, 1997). However, normal organogenesis seems to occur only when expansins are expressed in both outer and inner tissues (Pien *et al.*, 2001). Additionally, this expansin-induced organogenesis was only reported in tobacco SAMs with undisrupted auxin transport (Pien *et al.*, 2001). Therefore, it cannot be excluded that expansins only enhance the effect of other inductive signals including auxin.

Pectin modifications may also regulate the mechanical properties of cell walls. A local increase of pectin de-methylesterification found at incipient primordia in Arabidopsis has been proposed to be important for organ initiation (Peaucelle *et al.*, 2008). However, local pectin methyl esterase (PME) application at the *pin1* mutant SAMs triggers the formation of arrested, abnormal primordia, suggesting that pectin modifications occur downstream of auxin action (Braybrook and Peaucelle, 2013).

How could pectin modifications affect organ initiation? Using micro-indentation methods, pectin de-methylesterification was found to correlate with softer meristematic regions (Peaucelle *et al.*, 2011). Measurements seemed to indicate that this softening occurs exclusively in the inner tissues before primordium outgrowth. The softening in the outer layer was detected only after the primordium bulging. This suggests that pectin-mediated mechanical changes may be first initiated in the inner tissues, in agreement with model 2. However, the relationship between pectin de-methylesterification and cell wall expansion is uncertain. Pectin de-methylesterification was shown to decrease wall stiffness in Arabidopsis SAM, hypocotyl, and gynoecium (Peaucelle *et al.*, 2011, 2015; Andres-Robin *et al.*, 2018). In contradiction to this, higher pectin methylesterification has been linked to faster growth and softer cell walls in the pollen tube and in the root (reviewed in Palin and Geitmann, 2012; Bidhendi and Geitmann, 2016). Suprisingly, a recent study demonstrates that it is true also in the case of the Arabidopsis hypocotyl (Bou Daher *et al.*, 2018). These contradictory data may indicate that the relationship between pectin de-methylesterification, cell wall mechanics, and cell growth is indirect and depends on many additional factors, such as calcium content (Peaucelle *et al.*, 2008), hydration (Bidhendi and Geitmann, 2016), or pH (Hocq *et al.*, 2017). Another possible explanation may come from the fact that micro-indentation methods, including atomic force microscopy (AFM), are sensitive to cell and organ geometry (Routier-Kierzkowska *et al.*, 2012). Further investigations of the role of internal layers in growth regulation require detailed mechanical models for data interpretation. The relationship

between pectin modifications and expansion could be directly verified by simultaneous live-imaging of growth and pectin markers (Anderson *et al.*, 2012).

Auxin could also drive organ initiation via the regulation of cortical microtubule arrangement which controls the deposition of cellulose microfibrils in the cell walls (Ehrhardt and Shaw, 2006). A disorganized microtubule network was observed in Arabidopsis inflorescence meristem prior to the apparent outgrowth of flower primordia (Sassi *et al.*, 2014). In agreement, unaligned cellulose in the cell wall and isotropic growth are associated with the extensive outgrowth of floral primordia (Nelson, 1990; Reddy *et al.*, 2004; Kwiatkowska, 2006). However, microtubule orientation controls growth directionality but is not thought to affect the growth rate (Baskin, 2005). A recent study implies that disorganized microtubules and isotropic cell wall structure *per se* do not lead to an increase of cell growth rates necessary for primordium outgrowth (Armezzani *et al.*, 2018). In numerically modeled shoot apices, the growth rate in cells with isotropic walls is reduced compared with cells with anisotropic walls, suggesting that the reorganization of cell wall structure during organogenesis needs to be coupled with an increase in cell wall extensibility, as has been previously postulated (Fleming *et al.*, 1997; Reinhardt *et al.*, 1998; Pien *et al.*, 2001). Without a detailed quantitative analysis of cell growth, microtubule organization, and auxin accumulation patterns, it remains unclear whether microtubule reorganization is a cause or a consequence of auxin-induced changes in cell growth (Baskin, 2015; Schopfer and Palme, 2016). Auxin can trigger rapid growth via cell wall loosening; it is, therefore, possible that microtubules respond directly to growth-dependent changes in mechanical stresses (Fischer and Schopfer, 1997; Landrein and Hamant, 2013).

Does the pivotal role of auxin in organ initiation invalidate the models based on global tissue mechanics, such as the buckling model (model 3)? Most of the current data seems to suggest so. The generation of local auxin maxima precedes any morphological changes at the meristem surface (Reinhardt *et al.*, 2003; Bayer *et al.*, 2009), thus, it is unlikely that auxin maxima result from the mechanical stresses developed at the buckling surface (Newell and Shipman, 2005). Alternatively, the auxin-based mechanism, where local auxin maxima give rise to local surface deformation, was proposed to agree with the mechanism whereby growth-derived compressive stress initiate surface buckling (Newell *et al.*, 2008). In fact, mechanical stress can contribute to the auxin distribution via affecting PIN1 polarity and, thus, provide a feedback loop between auxin, growth, and mechanical stress (Heisler *et al.*, 2010; Nakayama *et al.*, 2012). Nonetheless, a prerequisite for buckling is the presence of in-plane compressive stresses which, at least up to now, has been found only in sunflower inflorescence meristem (Dumais and Steele, 2000; Dumais, 2007). A local increase in growth rates at the site of primordia initiation could result in compressive stresses around the young organ. This compression, rather than inducing true buckling, could, in turn, control the localization of boundary regulators (Landrein *et al.*, 2015).

As a final note, recently it has been shown that Arabidopsis stipules (organs located at the base of the leaf) initiate from a small number of cells located exclusively in the epidermis (Vuolo *et al.*, 2018). Increasing the number of founder cells in the *lmi1* mutant leads to the transformation of the stipules into leaf-like structures. Interestingly, this increase is always associated with the recruitment of cells from internal tissues. This suggests that both epidermal and internal tissue layers are required for normal organogenesis, but organ initiation can happen without any physical input from internal layers.

Biomechanical aspects of adaxial–abaxial leaf patterning

After organ initiation, the adaxial–abaxial polarity (or dorsiventral symmetry) is established. It is best understood in the case of leaves or sepals, and is crucial for their subsequent lateral expansion into planar structures (Waites and Hudson, 1995). This process involves a transcriptional regulatory network of genes that promotes adaxial and abaxial fates (Maugarny-Calès and Laufs, 2018). The dorsiventral symmetry is evident not only at later developmental stages in the differential distribution of specialized cells, such as trichomes (mostly adaxial side) or stomata (abaxial side), but also at very early stages by differential growth patterns at both sides of the primordia. In both early leaves and sepals, the growth rate is much higher at the abaxial primordium side than at the adaxial side (Barbier de Reuille *et al.*, 2015; McKim *et al.*, 2017).

How could such differential growth be established and how is it relevant for the generation of planar organ shape? Surgical isolation of the incipient primordium from the SAM leads to the radialization of the leaf, suggesting that the SAM produces a signal specifying adaxial–abaxial patterning (Sussex, 1951; Reinhardt, 2005). However, the molecular identity of this signal remains unknown. Recently, auxin was proposed to play a role in leaf adaxial–abaxial polarity establishment. Active transport of auxin from the primordium toward the SAM leads to the generation of the transient low-auxin zone in the adaxial side (Qi *et al.*, 2014). As auxin is known to modulate cell wall mechanics (Cleland, 1971; Edelmann and Kutschera, 1993; Braybrook and Peaucelle, 2013), an asymmetry in auxin distribution within the primordium might account for faster growth in the abaxial side. Indeed, using AFM, Qi *et al.* (2017) measured a significant difference in elasticity between adaxial and abaxial sides of leaf primordia in tomato. The abaxial side was softer compared with the adaxial side, which seems to be related to the higher de-methylesterification status of the wall pectins on this side, consistent with previous observations in the shoot apex (Peaucelle *et al.*, 2011). Computational modeling suggests that such mechanical difference would be sufficient for primordium flattening (Qi *et al.*, 2017). However, this scenario seems to be contradicted by a recent model of the same process where softer regions specified in the same way as by Qi and collaborators grow faster, thus failing to flatten the early primordium (Coen and Kennaway, 2018). Importantly, a recent quantitative analysis of auxin sensing in early leaf primordia argues against the proposed role of auxin in the establishment of leaf dorsoventrality (Bhatia *et al.*, 2019). Additionally, leaf and sepal primordia are flattened and pre-patterned by specific gene expression from their initiation (Barbier de Reuille *et al.*, 2015; Caggiano *et al.*,

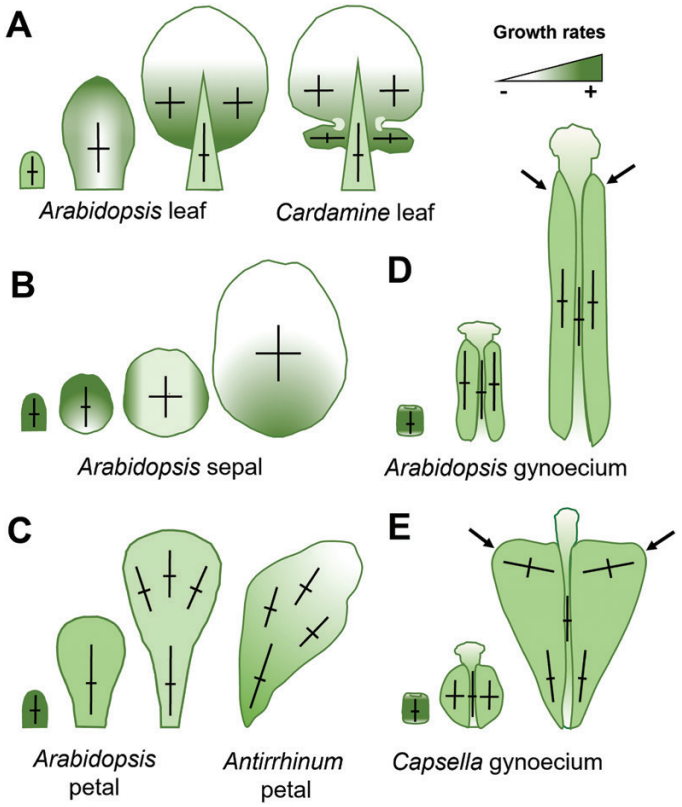

Fig. 3. Schematic representation of post-initiation surface growth patterns in shoot organs. (A) In Arabidopsis, an early leaf primordium grows rapidly along its main axis. During lamina initiation, growth is highest close to the leaf margins, and later decreases progressively from the tip to the base. After differentiation, the leaf blade tends to extend isotopically and the petiole/midrib more anisotropically (Fox *et al.*, 2018). In complex leaves (e.g. *Cardamine hirsuta*), anisotropic growth increases at the marginal protrusion and is restricted at the adjacent sinuses (Vlad *et al.*, 2014). (B) In Arabidopsis sepals, after an early fast elongation, growth rates decrease in the proximal regions. Later, growth becomes isotropic, with high growth rates observed only in cells located close to the lateral margins. Finally, a basipetal gradient of growth is established that restricts growth to more proximal regions of the sepal (Hervieux *et al.*, 2016). (C) Petal growth is relatively homogenous and anisotropic, with growth rates progressively decreasing during development. At later stages, growth is aligned along the main axis of the organ in proximal regions, and fan-out in more areas (Rolland-Lagan *et al.*, 2003; Sauret-Güeto *et al.*, 2013). (D) Throughout the development of Arabidopsis gynoecium, the growth is relatively uniform and anisotropic along the main organ axis, with growth rates progressively decreasing over time. (E) In *Capsella*, growth patterns are similar to those of Arabidopsis, except for valves, where growth becomes isotropic during the middle phase of development. At later stages, valve cells located near the base grow along the longitudinal axis, while cells in more distal regions elongate diagonally (Eldridge *et al.*, 2016). Crosses represent the principal directions of growth. The green scale indicates growth rates. Arrows indicate valves.

2017; McKim *et al.*, 2017). Softening of cell walls in the abaxial side of the primordium may, therefore, be independent of auxin and not be important for organ lateral expansion. Instead, it may be needed for the fast elongation of the primordium in the proximo-distal orientation, leading to its bending toward the meristem at early stages of development (Barbier de Reuille *et al.*, 2015; McKim *et al.*, 2017). Further observations of growth patterns combined with structural and mechanical anisotropy of cell walls are needed to discriminate between these possibilities.

Post-initiation growth of lateral organs

After initiation, growth patterns vary depending on organ type, size, and shape. Soon after emergence of the leaf primordium, it starts expanding along the medio-lateral axis of the future lamina (Fig. 3A). At this early stage, rapidly dividing and fast-growing cells are preferentially located close to the margin of the primordium (Donnelly *et al.*, 1999; Vuolo *et al.*, 2018), associated with the activity of the marginal meristem, also referred to as a marginal 'blastozone' (Hagemann and Gleissberg, 1996; Alvarez *et al.*, 2016). Subsequently, growth and cell proliferation become more dispersed within the leaf blade (Poethig and Sussex, 1985; Donnelly *et al.*, 1999; Kuchen *et al.*, 2012). In most model species, including Arabidopsis, tomato, tobacco, and maize, a basipetal gradient of growth and proliferation is progressively established in the leaf blade (Avery, 1933; Nath *et al.*, 2003; Ori *et al.*, 2007; Kuchen *et al.*, 2012; Nelissen *et al.*, 2012; Fox *et al.*, 2018). It is associated with faster cellular differentiation in more distal parts of the leaf (Donnelly *et al.*, 1999; Kazama *et al.*, 2010; Andriankaja *et al.*, 2012). However, such a basipetal gradient of growth is not a common feature of all leaves, as in many species different growth gradients are observed (Das Gupta and Nath, 2015). Soon after the differentiation of various parts of the leaf, the leaf blade tends to grow more isotopically (equally in all directions) as compared with the midrib and petiole, which tend to elongate along the proximo-distal axis (Ichihashi *et al.*, 2011; Bringmann and Bergmann, 2017; Fox *et al.*, 2018). After cell division arrest, a modified cell cycle leads to endoreplication (DNA replication without cell division) which consequently leads to differentiation into specific cell types often associated with an increase in cell size (i.e. pavement cells, or trichomes). Specialized epidermal cells, called meristemoids, keep proliferating for longer compared with the surrounding pavement cells (Andriankaja *et al.*, 2012). The final size of the leaf seems to be determined by cell number rather than cell size (Gázquez and Beemster, 2017).

Leaves are very variable in shape, ranging from simple, serrated, lobed to compound. This shape complexity is a consequence of spatio-temporal modulation of the marginal meristem activity (Bar and Ori, 2015; Rast-Somssich *et al.*, 2015; Alvarez *et al.*, 2016). The initiation of marginal leaf structures, such as lobes and leaflets, is determined by an auxin-based patterning mechanism (Barkoulas *et al.*, 2008; Bilsborough *et al.*, 2011), and their outgrowth results from the differential growth at the leaf margin (Nikovics *et al.*, 2006; Vlad *et al.*, 2014). During the initiation of marginal protrusions, cell growth increases at future protrusion tips, while it is restricted at the adjacent sinuses (Malinowski *et al.*, 2011; Vlad *et al.*, 2014). Additionally, cell growth is mainly oriented along the axis of outgrowths (Fig. 3A) (Vlad *et al.*, 2014).

Growth patterns in the Arabidopsis sepals share some similar features with simple leaves (Fig. 3B). After sepal initiation, cellular growth rates are very high, and growth is oriented along the proximo-distal axis of the organ (Sauret-Güeto, *et al.*, 2013; Hervieux *et al.*, 2016; McKim *et al.*, 2017). Cell growth rates first decrease in the more proximal regions of the developing sepal. Subsequently, fast-growing cells become restricted to the

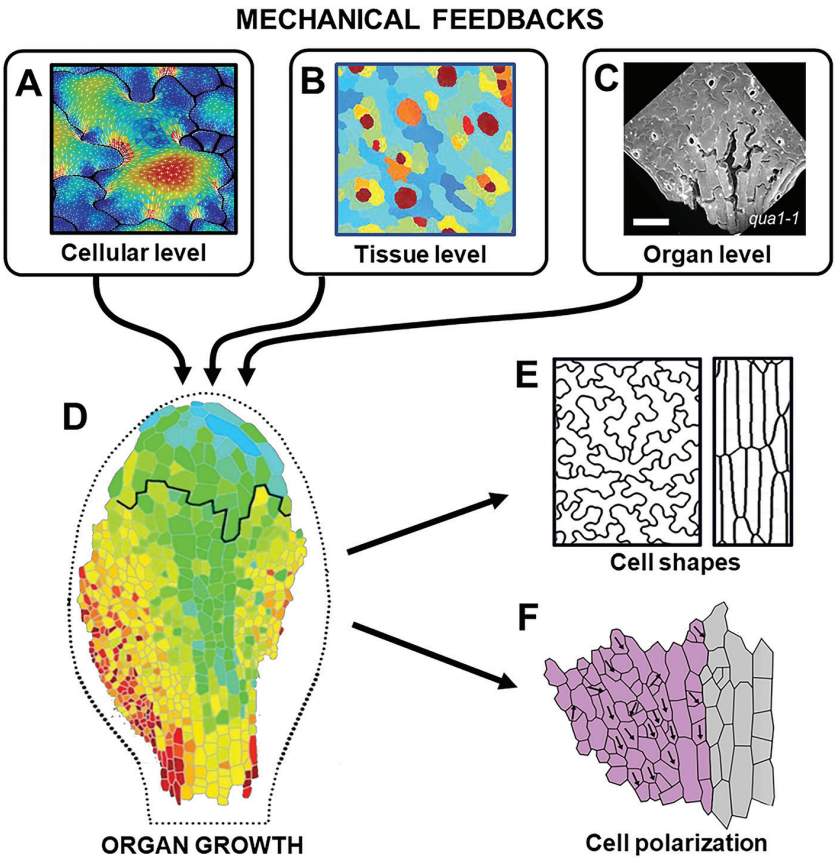

Fig. 4. Mechanical regulation of post-initiation organ growth. Mechanical feedbacks at (A) cellular (modified from Sapala *et al.*, 2018); (B) tissue; (C) and organ (modified from Verger *et al.*, 2018) levels regulate (D) growth of lateral organs (modified from Fox *et al.*, 2018). In turn, growth at the organ level can influence (E) individual cell shape (modified from Sapala *et al.*, 2018); and (F) cell or tissue polarization (modified from Current Biology 27, Bringmann M, Bergmann DC. Tissue-wide mechanical forces influence the polarity of stomatal stem cells in Arabidopsis. 877–883. Copyright (2017), with permission from Elsevier.

regions located close to lateral margins (Hervieux *et al.*, 2016; Tsugawa *et al.*, 2017). Relatively early (3–4 days after sepal initiation), growth becomes isotropic throughout the developing sepal. As in the leaves, a basipetal gradient of growth and proliferation is progressively established, but the slow-growing midrib and petiole observed in leaves are absent in sepals (Hervieux *et al.*, 2016). Instead, many epidermal cells stop dividing, endoreplicate, and massively increase in size, giving rise to giant cells (Roeder *et al.*, 2010; Tauriello *et al.*, 2015).

The growth of internal floral organs is less well understood, as they are not easily accessible for live-imaging. We will focus here on petal and gynoecium growth data which were inferred from clonal analysis (Rolland-Lagan *et al.*, 2003; Sauret-Güeto *et al.*, 2013; Eldridge *et al.*, 2016). At early stages of Arabidopsis petal development, cellular growth and division rates are relatively high. As the petal extends, growth slows down progressively (Fig. 3C) (Anastasiou and Lenhard, 2008; Sauret-Güeto *et al.*, 2013). The shapes of clonal sectors suggest that growth is anisotropic and oriented mainly along the proximo-distal axis of the petal from the earliest stages of its development. In proximal regions, clonal sector axes are parallel to each other, whereas they tend to fan out in the more distal regions (Sauret-Güeto *et al.*, 2013). In contrast to leaves, growth seems to be distributed rather uniformly over the whole petals, as indicated by the low variability in clone sizes (Sauret-Güeto *et al.*, 2013). Unlike bilaterally symmetrical petals in Arabidopsis, dorsal petals in *Antirrhinum* are asymmetrical. A key aspect of this asymmetry seems to depend on the directionality of growth rather than regional differences in growth rates (Rolland-Lagan *et al.*, 2003; Raczyńska-Szajgin and Nakielski, 2014). Divergent patterns of growth anisotropies in the petal distal domain are probably controlled by auxin, which has a broader distribution in the petal distal margin compared with the leaf primordium (Kuchen *et al.*, 2012; Sauret-Güeto *et al.*, 2013).

The gynoecium in Brassicaceae gives rise to the fruit called the silique and is composed of specialized parts that ensure seed development and their release upon maturity. The lateral parts, called valves, are fused to the replum via the valve margin. The style topped with the papillae is located at the tip of the gynoecium (Roeder and Yanofsky, 2006). The growth pattern in two Brassicaceae species with contrasting fruit shapes (i.e. elongated in Arabidopsis and heart-shaped in *Capsella rubella*) has recently been monitored using clonal analysis (Eldridge *et al.*, 2016). The development of the gynoecium can be divided into three phases: early, middle, and late (Fig. 3D, E). In Arabidopsis, all three phases are characterized by relatively uniform, anisotropic growth along the gynoecium axis, with growth rates progressively decreasing over time (Fig. 3D) (Eldridge *et al.*, 2016). In *Capsella*, growth patterns in the style and replum are comparable with those of Arabidopsis (Fig. 3E). In contrast,

growth in valves tends to be more isotropic during the middle stage. In the late stage, cells located close to the base of the valve grow along the replum axis, while cells at its top extend diagonally (Fig. 3D, E).

Clonal analysis proved to be useful in extending our understanding of organ growth. It must, however, be noted that this method may lead to some misinterpretations. First, the spatio-temporal resolution is relatively low, which may lead to averaging of some subtle, short-lasting but important differences in growth rates or directionalities. For example, anisotropic growth that changes its orientation over time may lead to the development of isotropic clones. Secondly, the final elongated shape of the clone may not necessarily reflect anisotropic growth, if the initial cell was already elongated before induction. Time-lapse imaging at cellular resolution should be the primary choice to avoid these potential misinterpretations. As progress in live imaging has been rapid in recent years (Schiessl *et al.*, 2012; Vlad *et al.*, 2014; Hervieux *et al.*, 2016; Fox *et al.*, 2018; Jackson *et al.*, 2019), we should expect that, in the near future, such an approach will be extended to even more challenging organs.

Mechanics of post-initiation organ growth

As a consequence of the mechanical continuum of plant cell walls, cell deformation depends not only on local cellular properties but also on the constraints imposed by their surroundings. Local differences in growth parameters can create mechanical conflicts that modify stress distribution in a small region, and therefore affect growth of the neighboring cells (Coen and Rebocho, 2016; Rebocho *et al.*, 2017). Those conflicts can arise at the cellular, tissue, or organ levels due to spatial variation in growth rates and orientations, cell wall mechanical properties, turgor pressure, and/or cell geometries (Fig. 4). Note that this kind of local influence does not require an active feedback (i.e. sensing stresses and reacting to them) but results solely from the fact that cell walls are connected to each other.

Majda *et al.* (2017) provide an example of the cellular mechanical interaction at the cell wall level, which arises during the initiation of leaf pavement cells. Using a combination of AFM measurements and immunolabeling, the authors show that both the composition and mechanical properties of anticlinal cell walls of adjacent cells are heterogeneous. A computational model suggests that the resulting mechano-chemical polarization of the anticlinal walls is important for initial cell wall bending under tension, a first step in the creation of the pavement cell lobe (Majda *et al.*, 2017). Alternatively, a recent model of the lobe initiation proposes that the mechanical shaping of the pavement cells rather relies on stiffening of the cell wall in the periclinal walls, following an active feedback mechanism (Bidhendi *et al.*, 2019, Preprint). Once pavement cells start to expand in size, active local reinforcement of the periclinal walls seems more relevant for shape acquisition (Sampathkumar *et al.*, 2014) as cells aim to minimalize the stresses at the level of the individual cell wall facing the environment (Sapala *et al.*, 2018).

Local growth differences between individual cells seem to play an important role in organogenesis. Using sepals as a model system, Hong *et al.* (2016) suggest that variability in cellular growth can contribute to reproducible organ shapes. Local mechanical feedbacks between cells probably decrease the differences between the growth rates of neighboring cells. Mechanical modeling shows that this feedback leads to spatio-temporal averaging of cellular growth variability, which may be required for the precise control of organ size and shape (Hervieux *et al.*, 2017). Growth variability could result from local differences in several parameters, such as turgor pressure, cell geometry, and wall mechanical properties. Measuring all these parameters in the same cells presents a technical challenge. Experimental data using micro-indentation techniques suggest that both cell wall mechanical properties and turgor pressure can differ between neighboring cells (Beauzamy *et al.*, 2015*a*; Hong *et al.*, 2016; Long *et al.*, 2018, Preprint). However, computer simulations indicate that the stiffness measured with such techniques correlates rather with cellular geometry and may not necessarily result from differences in material properties or pressure (Mosca *et al.*, 2017). Interestingly, when ignoring local growth variability related to the expansion of specialized cells (e.g. stomata), relatively smooth gradients of cellular growth can be observed along many organs even if individual cells differ in size and shape (Kuchen *et al.*, 2012; Barbier de Reuille *et al.*, 2015; Fox *et al.*, 2018; Vuolo *et al.*, 2018; Kierzkowski and Routier-Kierzkowska, 2019). The final organ size, shape, and growth patterns seem little affected by variation in individual cell sizes (Roeder *et al.*, 2010; Hervieux *et al.*, 2016; Schwarz and Roeder, 2016), which emphasizes the importance of supracellular factors and supports the accuracy of organismal theory for plant morphogenesis (Kaplan and Hagemann 1991). Combining different measurement methods and modeling should bring us closer to understanding the role of local cell growth variability for the control of growth at the level of organs.

In addition to cellular and tissue mechanical interactions, organ development can also be controlled by mechanical feedbacks at the organ level. These feedbacks may depend on the mechanical stresses resulting from geometry of an organ (Dumais and Steele, 2000; Hamant *et al.*, 2008), mechanical properties of tissues (Kutschera and Niklas, 2007), and/or tissue-dependent growth (Burian *et al.*, 2013). These stresses can affect cortical microtubules which have been shown to align along maximal tensile stress (Hejnowicz *et al.*, 2000; Hamant *et al.*, 2008; Bozorg *et al.*, 2014), and influence growth directionality. Such global feedbacks have been proposed to act as an organ shape-sensing mechanism (Green, 1999). Accordingly, mechanical conflicts between fast-growing basal and slow-growing apical regions in Arabidopsis sepals have been suggested to induce anisotropic tensile stress (Hervieux *et al.*, 2016). This stress would cause microtubule alignment and subsequently restrict the lateral expansion in the intermediate zone. Therefore, global mechanical conflicts may contribute to the final sepal shape by restricting regional growth. It should be noted that such a global mechanism could work only if cells were able to sense tissue-wide stresses, rather than stresses resulting from their own turgor pressure. Mechanical simulations in 3D are needed to determine the conditions in which tissue-wide stress could overcome local stresses generated by individual cells.

Mechanical coordination of growth requires cell adhesion. Taking advantage of a cell adhesion defect mutant in Arabidopsis, Verger *et al.* (2018) deduce stress patterns at the level of the growing organs. In relatively slow-growing tissues (e.g. close to the shoot apex), cell adhesions defects of the *quasimodo* mutant correlate with the cell-level stresses related to organ geometry. In contrast, in fast-growing tissues (e.g. dark-grown hypocotyl), cell-level stresses seem to be overcome by tissue-level stress. As the loss of epidermal continuity in a *quasimodo* mutant hampers supracellular alignment of cortical microtubules, this confirms that propagation of tensile stresses at the level of tissue is enabled by cell–cell adhesion. Interestingly, the cell adhesion defects were detected at the transition zone between differentially growing tissues (i.e. at the junction between isotropically growing leaf blade and elongating petiole) (Verger *et al.*, 2018), suggesting that the conflict between isotropic and anisotropic growth would be sufficient to bias stress direction at the boundary. This observation supports the idea that regional mechanical feedback between fast- and slow-growing tissues could regulate their growth and shape via mechanical feedback (Hervieux *et al.*, 2016). It would be very interesting to verify whether the patterns of cell adhesion defect indeed match with the predicted zone of tensile stresses and mechanical conflict in sepals.

Mechanical conflicts may also arise between tissue layers in developing organs. At the SAM, the outermost layer is believed to be under tension generated by the internal tissue (Kutschera and Niklas, 2007; Kierzkowski *et al.*, 2012; Beauzamy *et al.*, 2015*b*). Within an organ, tension in one layer (e.g. the epidermis) can only exist if other layers (in this case, ground tissues) are compressed. During leaf expansion, however, intercellular gas spaces progressively develop in the ground tissue (Wuyts *et al.*, 2010; Earles *et al.*, 2018), suggesting that internal layers may not be under compression. In consequence, the epidermis in expanding leaves may not be under tension as observed at the SAM. Outer tissue layers may, therefore, either drive or restrict plant growth (Savaldi-Goldstein *et al.*, 2007) depending on the developmental context. Interestingly, the development of intercellular spaces is not equal within the leaf. They are more common in the leaf blade which tends to grow more isotopically, while being nearly absent in elongating petiole (Fox *et al.*, 2018). This difference in subepidermal cell connectivity may suggest that the epidermis plays a different role in controlling growth even within different regions of the same organ, for example driving growth in the leaf blade and restricting it in the petiole. Layer-specific modulation of growth and tissue adhesion should help in clarifying these questions.

Stress generated during organ expansion can also feed back on growth behavior of individual cells. Stress patterns at the cellular level depend on their geometry (Kierzkowski and Routier-Kierzkowska, 2019). Cells can elongate in one direction without compromising their mechanical stability as the maximal stress will be constant and related to the diameter of the cell. However, growth in many lateral organs (i.e. expanding leaf blade) is isotropic, preventing the cells from elongating in a unique direction (Fox *et al.*, 2018). Using a combination of modeling and experimentation, Sapala and co-workers recently demonstrated that in pavement cells, increasing only the length or number of lobes does not result in an increase in stress. The development of lobes in pavement cells, therefore, seems an efficient strategy enabling cells to grow in all directions while keeping mechanical stresses low (Sapala *et al.*, 2018).

Tissue-wide mechanical stresses do not only impact how cells expand but may even influence cell polarity (Asnacios and Hamant, 2012). The orientation and magnitude of the mechanical stress have been suggested to influence the polarization of the PIN1 auxin efflux carrier (Heisler *et al.*, 2010; Nakayama *et al.*, 2012). More recently, mechanical feedback has also been proposed to control cell polarization, leading to asymmetric divisions in stomatal stem cells in leaf epidermis (Bringmann and Bergmann, 2017). The polarization of BREVIS RADIX LIKE2 (BRXL2) protein can be altered by inducing changes in the mechanical stress pattern due to leaf stretching or cell ablations. Interestingly, the response of neither PIN1 nor BRXL2 to mechanical stress is mediated by microtubules (Heisler *et al.*, 2010; Bringmann and Bergmann, 2017), which play a key role in plant mechanosensing (reviewed in Landrein and Hamant, 2013). Therefore, how tissue mechanical stresses are translated into the polarized localization of proteins in individual cells currently remains a mystery.

Conclusions

Mechanics plays a crucial role in controlling plant growth and morphogenesis. While much progress has been made in plant biomechanics, there is still a long way to go until we can fully comprehend the precise interplay between physical forces and growth. Recent studies have provided improved spatio-temporal resolution growth data throughout organ development (Hervieux *et al.*, 2016), a comprehensive growth analysis of various cell layers (Fox *et al.*, 2018), and 3D data of cell volumes for topology analysis and lineage tracking (Vuolo *et al.*, 2018; Jackson *et al.*, 2019). The advancement of live-imaging and deep tissue imaging enables acquisition of quantitative cell resolution growth data in various organs and plant systems, which will continue to broaden our understanding of the universal principals underlying organogenesis. On the other hand, we currently witness remarkable advancements in the development of cutting-edge technologies such as micro-mechanical measurement methods (Milani *et al.*, 2011; Routier-Kierzkowska *et al.*, 2012; Sahaf and Sharon, 2016; Robinson *et al.*, 2017), image analysis software (Barbier de Reuille *et al.*, 2015), and computer modeling (Mosca *et al.*, 2017; Armezzani *et al.*, 2018; Bidhendi and Geitmann, 2018*a*, *b*; Robinson and Kuhlemeier, 2018; Sapala *et al.*, 2018). The future of biomechanics relies on the integration of these various approaches into a more interdisciplinary field. In this way, many of the published data on the regulation of growth (i.e. by hormones and environmental conditions) could be revisited from the biomechanical perspective.

Acknowledgements

We thank Dorota Kwiatkowska, Daniel Schoen, and Nicholas Brereton for comments on this manuscript. Research in the Kierzkowski lab and

the Routier-Kierzkowska lab is funded by Discovery Grants RN000758 and RN000787, respectively, from the Natural Sciences and Engineering Research Council of Canada. AB and NS are supported by the research grant SONATA BIS6 (2016/22/E/NZ3/00342) from the the National Science Centre, Poland. The funding sources were not involved in the design or content of this review.

References

Alvarez JP, Furumizu C, Efroni I, Eshed Y, Bowman JL. 2016. Active suppression of a leaf meristem orchestrates determinate leaf growth. eLife **5**, e15023.

Alvarez-Buylla ER, Benítez M, Corvera-Poiré A, *et al.* 2010. Flower development. The Arabidopsis Book **8**, 1–57.

Anastasiou E, Lenhard M. 2008. Control of plant organ size. In: Bögre L, Beemster G, eds. Plant growth signaling. Berlin: Springer, 22–45.

Anderson CT, Wallace IS, Somerville CR. 2012. Metabolic click-labeling with a fucose analog reveals pectin delivery, architecture, and dynamics in *Arabidopsis* cell walls. Proceedings of the National Academy of Sciences, USA **109**, 1329–1334.

Andres-Robin A, Reymond M, Dupire A, *et al.* 2018. Evidence for the control of Arabidopsis gynoecium morphogenesis by ETTIN via cell wall dynamics. Plant Physiology **178**, 1222–1232.

Andriankaja M, Dhondt S, De Bodt S, *et al.* 2012. Exit from proliferation during leaf development in *Arabidopsis thaliana*: a not-so-gradual process. Developmental Cell **22**, 64–78.

Armezzani A, Abad U, Ali O, *et al.* 2018. Transcriptional induction of cell wall remodelling genes is coupled to microtubule-driven growth isotropy at the shoot apex in Arabidopsis. Development **145**, 1–55.

Asnacios A, Hamant O. 2012. The mechanics behind cell polarity. Trends in Cell Biology **22**, 584–591.

Avery GSJ. 1933. Structure and development of the tobacco leaf. American Journal of Botany **20**, 565–592.

Bar M, Ori N. 2015. Compound leaf development in model plant species. Current Opinion in Plant Biology **23**, 61–69.

Barbier de Reuille P, Routier-Kierzkowska A-L, Kierzkowski D, *et al.* 2015. MorphoGraphX: a platform for quantifying morphogenesis in 4D. eLife **4**, e05864.

Barkoulas M, Hay A, Kougioumoutzi E, Tsiantis M. 2008. A developmental framework for dissected leaf formation in the Arabidopsis relative *Cardamine hirsuta*. Nature Genetics **40**, 1136–1141.

Baskin TI. 2005. Anisotropic expansion of the plant cell wall. Annual Review of Cell and Developmental Biology **21**, 203–222.

Baskin TI. 2015. Auxin inhibits expansion rate independently of cortical microtubules. Trends in Plant Science **20**, 471–472.

Baskin TI, Jensen OE. 2013. On the role of stress anisotropy in the growth of stems. Journal of Experimental Botany **64**, 4697–4707.

Bassel GW, Smith RS. 2016. Quantifying morphogenesis in plants in 4D. Current Opinion in Plant Biology **29**, 87–94.

Bassel GW, Stamm P, Mosca G, Barbier de Reuille P, Gibbs DJ, Winter R, Janka A, Holdsworth MJ, Smith RS. 2014. Mechanical constraints imposed by 3D cellular geometry and arrangement modulate growth patterns in the Arabidopsis embryo. Proceedings of the National Academy of Sciences, USA **111**, 8685–8690.

Bayer EM, Smith RS, Mandel T, Nakayama N, Sauer M, Prusinkiewicz P, Kuhlemeier C. 2009. Integration of transport-based models for phyllotaxis and midvein formation. Genes & Development **23**, 373–384.

Beauzamy L, Derr J, Boudaoud A. 2015*a*. Quantifying hydrostatic pressure in plant cells by using indentation with an atomic force microscope. Biophysical Journal **108**, 2448–2456.

Beauzamy L, Louveaux M, Hamant O, Boudaoud A. 2015*b*. Mechanically, the shoot apical meristem of Arabidopsis behaves like a shell inflated by a pressure of about 1 MPa. Frontiers in Plant Science **6**, 1038.

Bhatia N, Ahl H, Jönsson H, Heisler MG. 2019. Quantitative analysis of auxin sensing in leaf primordia argues against proposed role in regulating leaf dorsoventrality. eLife **8**, e39298.

Bidhendi AJ, Altartouri B, Gosselin FP, Geitmann A. 2019. Mechanical stress initiates and sustains the morphogenesis of wavy leaf epidermal cells. bioRxiv. 563403. [Preprint].

Bidhendi AJ, Geitmann A. 2016. Relating the mechanics of the primary plant cell wall to morphogenesis. Journal of Experimental Botany **67**, 449–461.

Bidhendi AJ, Geitmann A. 2018*a*. Tensile testing of primary plant cells and tissues. In: Geitmann A, Gril J, eds. Plant biomechanics. From structure to function at multiple scales. Cham: Springer International Publishing, 321–347.

Bidhendi AJ, Geitmann A. 2018*b*. Finite element modeling of shape changes in plant cells. Plant Physiology **176**, 41–56.

Bilsborough GD, Runions A, Barkoulas M, Jenkins HW, Hasson A, Galinha C, Laufs P, Hay A, Prusinkiewicz P, Tsiantis M. 2011. Model for the regulation of *Arabidopsis thaliana* leaf margin development. Proceedings of the National Academy of Sciences, USA **108**, 3424–3429.

Bou Daher F, Chen Y, Bozorg B, Clough J, Jonsson H, Braybrook SA. 2018. Anisotropic growth is achieved through the additive mechanical effect of material anisotropy and elastic asymmetry. eLife **7**, e38161.

Bowman JL, Smyth DR, Meyerowitz EM. 1991. Genetic interactions among floral homeotic genes of Arabidopsis. Development **112**, 1–20.

Bozorg B, Krupinski P, Jönsson H. 2014. Stress and strain provide positional and directional cues in development. PLoS Computational Biology **10**, e1003410.

Braybrook SA, Jönsson H. 2016. Shifting foundations: the mechanical cell wall and development. Current Opinion in Plant Biology **29**, 115–120.

Braybrook SA, Peaucelle A. 2013. Mechano-chemical aspects of organ formation in *Arabidopsis thaliana*: the relationship between auxin and pectin. PLoS One **8**, e57813.

Breuil-Broyer S, Morel P, de Almeida-Engler J, Coustham V, Negrutiu I, Trehin C. 2004. High-resolution boundary analysis during *Arabidopsis thaliana* flower development. The Plant Journal **38**, 182–192.

Bringmann M, Bergmann DC. 2017. Tissue-wide mechanical forces influence the polarity of stomatal stem cells in Arabidopsis. Current Biology **27**, 877–883.

Burian A, Barbier de Reuille P, Kuhlemeier C. 2016. Patterns of stem cell divisions contribute to plant longevity. Current Biology **26**, 1–10.

Burian A, Ludynia M, Uyttewaal M, Traas J, Boudaoud A, Hamant O, Kwiatkowska D. 2013. A correlative microscopy approach relates microtubule behaviour, local organ geometry, and cell growth at the Arabidopsis shoot apical meristem. Journal of Experimental Botany **64**, 5753–5767.

Caggiano MP, Yu X, Bhatia N, Larsson A, Ram H, Ohno CK, Sappl P, Meyerowitz EM, Jönsson H, Heisler MG. 2017. Cell type boundaries organize plant development. eLife **6**, e27421.

Clark SE. 1997. Organ formation at the vegetative shoot meristem. The Plant Cell **9**, 1067–1076.

Cleland R. 1971. Cell wall extension. Annual Review of Plant Physiology **22**, 197–222.

Coen E, Kennaway R. 2018. Early shaping of a leaf. Nature Plants **4**, 618–619.

Coen ES, Meyerowitz EM. 1991. The war of the whorls: genetic interactions controlling flower development. Nature **353**, 31–37.

Coen E, Rebocho AB. 2016. Resolving conflicts: modeling genetic control of plant morphogenesis. Developmental Cell **38**, 579–583.

Coen E, Rolland-Lagan A-G, Matthews M, Bangham JA, Prusinkiewicz P. 2004. The genetics of geometry. Proceedings of the National Academy of Sciences, USA **101**, 4728–35.

Cosgrove DJ. 2000. Expansive growth of plant cell walls. Plant Physiology and Biochemistry **38**, 109–124.

Cosgrove DJ. 2016. Plant cell wall extensibility: connecting plant cell growth with cell wall structure, mechanics, and the action of wall-modifying enzymes. Journal of Experimental Botany **67**, 463–476.

Cosgrove DJ. 2018. Diffuse growth of plant cell walls. Plant Physiology **176**, 16–27.

Das Gupta M, Nath U. 2015. Divergence in patterns of leaf growth polarity is associated with the expression divergence of miR396. The Plant Cell **27**, 2785–2799.

Donnelly PM, Bonetta D, Tsukaya H, Dengler RE, Dengler NG. 1999. Cell cycling and cell enlargement in developing leaves of Arabidopsis. Developmental Biology **215**, 407–419.

Dumais J. 2007. Can mechanics control pattern formation in plants? Current Opinion in Plant Biology **10**, 58–62.

Dumais J, Steele CR. 2000. New evidence for the role of mechanical forces in the shoot apical meristem. Journal of Plant Growth Regulation **19**, 7–18.

Earles JM, Theroux-Rancourt G, Roddy AB, Gilbert ME, McElrone AJ, Brodersen CR. 2018. Beyond porosity: 3D leaf intercellular airspace traits that impact mesophyll conductance. Plant Physiology **178**, 148–162.

Edelmann HG, Kutschera U. 1993. Rapid auxin-induced enhancement of protein biosynthesis in rye coleoptiles. Journal of Plant Physiology **142**, 343–346.

Ehrhardt DW, Shaw SL. 2006. Microtubule dynamics and organization in the plant cortical array. Annual Review of Plant Biology **57**, 859–875.

Eldridge T, Łangowski Ł, Stacey N, *et al.* 2016. Fruit shape diversity in the Brassicaceae is generated by varying patterns of anisotropy. Development **143**, 3394–3406.

Fischer K, Schopfer P. 1997. Interaction of auxin, light, and mechanical stress in orienting microtubules in relation to tropic curvature in the epidermis of maize coleoptiles. Protoplasma **196**, 108–116.

Fleming AJ. 2006. The co-ordination of cell division, differentiation and morphogenesis in the shoot apical meristem: a perspective. Journal of Experimental Botany **57**, 25–32.

Fleming AJ, McQueen-Mason S, Mandel T, Kuhlemeier C. 1997. Induction of leaf primordia by the cell wall. Science **276**, 1415–1418.

Fox S, Southam P, Pantin F, *et al.* 2018. Spatiotemporal coordination of cell division and growth during organ morphogenesis. PLoS Biology **16**, e2005952.

Gázquez A, Beemster GTS. 2017. What determines organ size differences between species? A meta-analysis of the cellular basis. New Phytologist **215**, 299–308.

Green PB. 1999. Expression of pattern in plants: combining molecular and calculus-based biophysical paradigms. American Journal of Botany **86**, 1059–1076.

Green PB, Selker JML. 1991. Mutual alignments of cell walls, cellulose, and cytoskeletons: their role in meristems. In: Lloyd CW, ed.The cytoskeletal basis of plant growth and form. New York: Academic Press, 303–332.

Green PB, Steele CS, Rennich SC. 1996. Phyllotactic patterns: a biophysical mechanism for their origin. Annals of Botany **77**, 515–527.

Hagemann W, Gleissberg S. 1996. Organogenetic capacity of leaves: the significance of marginal blastozones in angiosperms. Plant Systematics and Evolution **199**, 121–152.

Hamant O. 2017. Mechano-devo. Mechanisms of Development **145**, 2–9.

Hamant O, Heisler MG, Jönsson H, *et al.* 2008. Developmental patterning by mechanical signals in Arabidopsis. Science **322**, 1650–1655.

Heisler MG, Hamant O, Krupinski P, Uyttewaal M, Ohno C, Jönsson H, Traas J, Meyerowitz EM. 2010. Alignment between PIN1 polarity and microtubule orientation in the shoot apical meristem reveals a tight coupling between morphogenesis and auxin transport. PLoS Biology **8**, e1000516.

Heisler MG, Ohno C, Das P, Sieber P, Reddy GV, Long JA, Meyerowitz EM. 2005. Patterns of auxin transport and gene expression during primordium development revealed by live imaging of the Arabidopsis inflorescence meristem. Current Biology **15**, 1899–1911.

Hejnowicz Z, Rusin A, Rusin T. 2000. Tensile tissue stress affects the orientation of cortical microtubules in the epidermis of sunflower hypocotyl. Journal of Plant Growth Regulation **19**, 31–44.

Hervieux N, Dumond M, Sapala A, Smith RS, Boudaoud A, Hamant O, Hervieux N, Dumond M, Sapala A, Kierzkowski D. 2016. A mechanical feedback restricts sepal growth and shape in Arabidopsis. Current Biology **26**, 1019–1028.

Hervieux N, Tsugawa S, Fruleux A, *et al.* 2017. Mechanical shielding of rapidly growing cells buffers growth heterogeneity and contributes to organ shape reproducibility. Current Biology **27**, 3468–3479.e4.

Hocq L, Pelloux J, Lefebvre V. 2017. Connecting homogalacturonan-type pectin remodeling to acid growth. Trends in Plant Science **22**, 20–29.

Hofhuis H, Moulton D, Lessinnes T, *et al.* 2016. Morphomechanical innovation drives explosive seed dispersal. Cell **166**, 222–233.

Hong L, Dumond M, Tsugawa S, *et al.* 2016. Variable cell growth yields reproducible organ development through spatiotemporal averaging. Developmental Cell **38**, 15–32.

Ichihashi Y, Kawade K, Usami T, Horiguchi G, Takahashi T, Tsukaya H. 2011. Key proliferative activity in the junction between the leaf blade and leaf petiole of Arabidopsis. Plant Physiology **157**, 1151–1162.

Ingram G, Mähönen AP. 2018. Editorial overview: growth and development. Current Opinion in Plant Biology **41**, iii–iiv.

Jackson MDB, Duran-Nebreda S, Kierzkowski D, Strauss S, Xu H, Landrein B, Hamant O, Smith RS, Johnston IG, Bassel GW. 2019. Global topological order emerges through local mechanical control of cell divisions in the Arabidopsis shoot apical meristem. Cell Systems **8**, 53–65.e3.

Kaplan DR, Hagemann W. 1991. The relationship of cell and organism in vascular plants: are cells the building blocks of plant form? BioScience **41**, 693–703.

Kazama T, Ichihashi Y, Murata S, Tsukaya H. 2010. The mechanism of cell cycle arrest front progression explained by a KLUH/CYP78A5-dependent mobile growth factor in developing leaves of *Arabidopsis thaliana*. Plant & Cell Physiology **51**, 1046–1054.

Kierzkowski D, Lenhard M, Smith R, Kuhlemeier C. 2013. Interaction between meristem tissue layers controls phyllotaxis. Developmental Cell **26**, 616–628.

Kierzkowski D, Nakayama N, Routier-Kierzkowska AL, Weber A, Bayer E, Schorderet M, Reinhardt D, Kuhlemeier C, Smith RS. 2012. Elastic domains regulate growth and organogenesis in the plant shoot apical meristem. Science **335**, 1096–1099.

Kierzkowski D, Routier-Kierzkowska AL. 2019. Cellular basis of growth in plants: geometry matters. Current Opinion in Plant Biology **47**, 56–63.

Kuchen EE, Fox S, de Reuille PB, *et al.* 2012. Generation of leaf shape through early patterns of growth and tissue polarity. Science **335**, 1092–1096.

Kutschera U, Niklas KJ. 2007. The epidermal-growth-control theory of stem elongation: an old and a new perspective. Journal of Plant Physiology **164**, 1395–1409.

Kwiatkowska D. 2004. Structural integration at the shoot apical meristem: models, measurements, and experiments. American Journal of Botany **91**, 1277–1293.

Kwiatkowska D. 2006. Flower primordium formation at the Arabidopsis shoot apex: quantitative analysis of surface geometry and growth. Journal of Experimental Botany **57**, 571–580.

Kwiatkowska D, Dumais J. 2003. Growth and morphogenesis at the vegetative shoot apex of *Anagallis arvensis* L. Journal of Experimental Botany **54**, 1585–1595.

Kwiatkowska D, Routier-Kierzkowska AL. 2009. Morphogenesis at the inflorescence shoot apex of *Anagallis arvensis*: surface geometry and growth in comparison with the vegetative shoot. Journal of Experimental Botany **60**, 3407–3418.

Landrein B, Hamant O. 2013. How mechanical stress controls microtubule behavior and morphogenesis in plants: history, experiments and revisited theories. The Plant Journal **75**, 324–338.

Landrein B, Kiss A, Sassi M, *et al.* 2015. Mechanical stress contributes to the expression of the STM homeobox gene in Arabidopsis shoot meristems. eLife **4**, e07811.

Leyser O. 2018. Auxin signaling. Plant Physiology **176**, 465–479.

Long J, Barton MK. 2000. Initiation of axillary and floral meristems in Arabidopsis. Developmental Biology **218**, 341–353.

Long Y, Cheddadi I, Mirabet V, Dumond M, Godin C, Boudaoud A. 2018. Cellular heterogeneity in pressure and growth emerges from tissue topology and geometry. bioRxiv 334664. [Preprint].

Majda M, Grones P, Sintorn IM, *et al.* 2017. Mechanochemical polarization of contiguous cell walls shapes plant pavement cells. Developmental Cell **43**, 290–304.e4.

Malinowski R, Kasprzewska A, Fleming AJ. 2011. Targeted manipulation of leaf form via local growth repression. The Plant Journal **66**, 941–952.

Maugarny-Calès A, Laufs P. 2018. Getting leaves into shape: a molecular, cellular, environmental and evolutionary view. Development **145**, 1–16.

McKim SM, Routier-Kierzkowska AL, Monniaux M, Kierzkowski D, Pieper B, Smith RS, Tsiantis M, Hay A. 2017. Seasonal regulation of petal number. Plant Physiology **175**, 886–903.

McQueen-Mason SJ, Cosgrove DJ. 1995. Expansin mode of action on cell walls. Analysis of wall hydrolysis, stress relaxation, and binding. Plant Physiology **107**, 87–100.

Milani P, Gholamirad M, Traas J, Arnéodo A, Boudaoud A, Argoul F, Hamant O. 2011. In vivo analysis of local wall stiffness at the shoot apical meristem in Arabidopsis using atomic force microscopy. The Plant Journal **67**, 1116–1123.

Monniaux M, Pieper B, McKim SM, Routier-Kierzkowska A-L, Kierzkowski D, Smith RS, Hay A. 2018. The role of APETALA1 in petal number robustness. eLife **7**, e39399.

Mosca G, Sapala A, Strauss S, Routier-Kierzkowska AL, Smith RS. 2017. On the micro-indentation of plant cells in a tissue context. Physical Biology **14**, 015003.

Nakayama N, Smith RS, Mandel T, Robinson S, Kimura S, Boudaoud A, Kuhlemeier C. 2012. Mechanical regulation of auxin-mediated growth. Current Biology **22**, 1468–1476.

Nath U, Crawford BCW, Carpenter R, Coen E. 2003. Genetic control of surface curvature material and methods. Science **299**, 1404–1407.

Nelissen H, Rymen B, Jikumaru Y, Demuynck K, Van Lijsebettens M, Kamiya Y, Inzé D, Beemster GT. 2012. A local maximum in gibberellin levels regulates maize leaf growth by spatial control of cell division. Current Biology **22**, 1183–1187.

Nelson AJ. 1990. Net alignment of cellulose in the periclinal walls of the shoot apex surface cells in *Kalanchoe blossfeldiana*. II. Flower development. Canadian Journal of Botany **68**, 2678–2684.

Newell AC, Shipman PD. 2005. Plants and fibonacci. Journal of Statistical Physics **121**, 937–968.

Newell AC, Shipman PD, Sun Z. 2008. Phyllotaxis: cooperation and competition between mechanical and biochemical processes. Journal of Theoretical Biology **251**, 421–439.

Nikovics K, Blein T, Peaucelle A, Ishida T, Morin H, Aida M, Laufs P. 2006. The balance between the MIR164A and CUC2 genes controls leaf margin serration in Arabidopsis. The Plant Cell **18**, 2929–2945.

Ori N, Cohen AR, Etzioni A, *et al.* 2007. Regulation of LANCEOLATE by miR319 is required for compound-leaf development in tomato. Nature Genetics **39**, 787–791.

Overvoorde PJ, Okushima Y, Alonso JM, *et al.* 2005. Functional genomic analysis of the AUXIN/INDOLE-3-ACETIC ACID gene family members in *Arabidopsis thaliana*. The Plant Cell **17**, 3282–3300.

Palin R, Geitmann A. 2012. The role of pectin in plant morphogenesis. Bio Systems **109**, 397–402.

Peaucelle A, Braybrook SA, Le Guillou L, Bron E, Kuhlemeier C, Höfte H. 2011. Pectin-induced changes in cell wall mechanics underlie organ initiation in Arabidopsis. Current Biology **21**, 1720–1726.

Peaucelle A, Louvet R, Johansen JN, Höfte H, Laufs P, Pelloux J, Mouille G. 2008. Arabidopsis phyllotaxis is controlled by the methyl-esterification status of cell-wall pectins. Current Biology **18**, 1943–1948.

Peaucelle A, Wightman R, Höfte H. 2015. The control of growth symmetry breaking in the Arabidopsis hypocotyl. Current Biology **25**, 1746–1752.

Pelaz S, Tapia-López R, Alvarez-Buylla ER, Yanofsky MF. 2001. Conversion of leaves into petals in Arabidopsis. Current Biology **11**, 182–184.

Pien S, Wyrzykowska J, McQueen-Mason S, Smart C, Fleming A. 2001. Local expression of expansin induces the entire process of leaf development and modifies leaf shape. Proceedings of the National Academy of Sciences, USA **98**, 11812–11817.

Poethig RS, Sussex IM. 1985. The cellular parameters of leaf development in tobacco: a clonal analysis. Planta **165**, 170–184.

Qi J, Wang Y, Yu T, Cunha A, Wu B, Vernoux T, Meyerowitz E, Jiao Y. 2014. Auxin depletion from leaf primordia contributes to organ patterning. Proceedings of the National Academy of Sciences, USA **111**, 18769–18774.

Qi J, Wu B, Feng S, *et al.* 2017. Mechanical regulation of organ asymmetry in leaves. Nature Plants **3**, 724–733.

Raczyńska-Szajgin M, Nakielski J. 2014. Growth and cellular patterns in the petal epidermis of *Antirrhinum majus*: empirical studies. Annals of Botany **113**, 403–416.

Rast-Somssich MI, Broholm S, Jenkins H, *et al.* 2015. Alternate wiring of a KNOXI genetic network underlies differences in leaf development of *A. thaliana* and *C. hirsuta*. Genes & Development **29**, 2391–2404.

Rebocho X, Southam P, Kennaway R, Bangham A, Coen E. 2017. Generation of shape complexity through tissue conflicts. eLife **6**, e20156.

Reddy GV, Heisler MG, Ehrhardt DW, Meyerowitz EM. 2004. Real-time lineage analysis reveals oriented cell divisions associated with morphogenesis at the shoot apex of *Arabidopsis thaliana*. Development **131**, 4225–4237.

Reinhardt D. 2005. Phyllotaxis—a new chapter in an old tale about beauty and magic numbers. Current Opinion in Plant Biology **8**, 487–493.

Reinhardt D, Mandel T, Kuhlemeier C. 2000. Auxin regulates the initiation and radial position of plant lateral organs. The Plant Cell **12**, 507–518.

Reinhardt D, Pesce ER, Stieger P, Mandel T, Baltensperger K, Bennett M, Traas J, Friml J, Kuhlemeier C. 2003. Regulation of phyllotaxis by polar auxin transport. Nature **426**, 255–260.

Reinhardt D, Wittwer F, Mandel T, Kuhlemeier C. 1998. Localized upregulation of a new expansin gene predicts the site of leaf formation in the tomato meristem. The Plant Cell **10**, 1427–1437.

Robinson S, Huflejt M, Barbier de Reuille P, Braybrook SA, Schorderet M, Reinhardt D, Kuhlemeier C. 2017. An automated confocal micro-extensometer enables in vivo quantification of mechanical properties with cellular resolution. The Plant Cell **29**, 2959–2973.

Robinson S, Kuhlemeier C. 2018. Global compression reorients cortical microtubules in arabidopsis hypocotyl epidermis and promotes growth. Current Biology **28**, 1794–1802.e2.

Roeder AH, Chickarmane V, Cunha A, Obara B, Manjunath BS, Meyerowitz EM. 2010. Variability in the control of cell division underlies sepal epidermal patterning in *Arabidopsis thaliana*. PLoS Biology **8**, e1000367.

Roeder AH, Yanofsky MF. 2006. Fruit development in Arabidopsis. The Arabidopsis Book **4**, e0075.

Rolland-Lagan AG, Bangham JA, Coen E. 2003. Growth dynamics underlying petal shape and asymmetry. Nature **422**, 161–163.

Routier-Kierzkowska A-L, Runions A. 2018. Modeling plant biomechanics: an introduction. In: Geitmann A, Gril J, eds. Plant biomechanics. From structure to function at multiple scales. Cham: Springer International Publishing, 165–192.

Routier-Kierzkowska AL, Weber A, Kochova P, Felekis D, Nelson BJ, Kuhlemeier C, Smith RS. 2012. Cellular force microscopy for in vivo measurements of plant tissue mechanics. Plant physiology **158**, 1514–1522.

Sablowski R. 2015. Control of patterning, growth, and differentiation by floral organ identity genes. Journal of Experimental Botany **66**, 1065–1073.

Sahaf M, Sharon E. 2016. The rheology of a growing leaf: stress-induced changes in the mechanical properties of leaves. Journal of Experimental Botany **67**, 5509–5515.

Sampathkumar A, Krupinski P, Wightman R, Milani P, Berquand A, Boudaoud A, Hamant O, Jönsson H, Meyerowitz EM. 2014. Subcellular and supracellular mechanical stress prescribes cytoskeleton behavior in Arabidopsis cotyledon pavement cells. eLife **3**, e01967.

Sapala A, Runions A, Routier-Kierzkowska AL, *et al*. 2018. Why plants make puzzle cells, and how their shape emerges. eLife **7**, e32794.

Sassi M, Ali O, Boudon F, *et al.* 2014. An auxin-mediated shift toward growth isotropy promotes organ formation at the shoot meristem in Arabidopsis. Current Biology **24**, 2335–2342.

Sauret-Güeto S, Schiessl K, Bangham A, Sablowski R, Coen E. 2013. JAGGED controls Arabidopsis petal growth and shape by interacting with a divergent polarity field. PLoS Biology **11**, e1001550.

Savaldi-Goldstein S, Peto C, Chory J. 2007. The epidermis both drives and restricts plant shoot growth. Nature **446**, 199–202.

Schiessl K, Kausika S, Southam P, Bush M, Sablowski R. 2012. JAGGED controls growth anisotropy and coordination between cell size and cell cycle during plant organogenesis. Current Biology **22**, 1739–1746.

Schwarz EM, Roeder AHK. 2016. Transcriptomic effects of the cell cycle regulator LGO in Arabidopsis sepals. Frontiers in Plant Science **7**, 1744.

Selker JM, Steucek GL, Green PB. 1992. Biophysical mechanisms for morphogenetic progressions at the shoot apex. Developmental Biology **153**, 29–43.

Schopfer P, Palme K. 2016. Inhibition of cell expansion by rapid ABP1-mediated auxin effect on microtubules? A critical comment. Plant Physiology **170**, 23–25.

Smith RS, Guyomarc'h S, Mandel T, Reinhardt D, Kuhlemeier C, Prusinkiewicz P. 2006. A plausible model of phyllotaxis. Proceedings of the National Academy of Sciences, USA **103**, 1301–1306.

Smyth DR, Bowman JL, Meyerowitz EM. 1990. Early flower development in Arabídopsis. The Plant Cell **2**, 755–767.

Steeves T, Sussex IM. 1989. Patterns in plant development. Cambridge: Cambridge University Press.

Sussex IM. 1951. Experiments on the cause of dorsiventrality in leaves. Nature **167**, 651–652.

Takahashi K, Hayashi K, Kinoshita T. 2012. Auxin activates the plasma membrane H^+-ATPase by phosphorylation during hypocotyl elongation in Arabidopsis. Plant Physiology **159**, 632–641.

Tauriello G, Meyer HM, Smith RS, Koumoutsakos P, Roeder AH. 2015. Variability and constancy in cellular growth of Arabidopsis sepals. Plant Physiology **169**, 2342–2358.

Tsugawa S, Hervieux N, Kierzkowski D, Routier-Kierzkowska AL, Sapala A, Hamant O, Smith RS, Roeder AHK, Boudaoud A, Li CB. 2017. Clones of cells switch from reduction to enhancement of size variability in Arabidopsis sepals. Development **144**, 4398–4405.

Verger S, Long Y, Boudaoud A, Hamant O. 2018. A tension–adhesion feedback loop in plant epidermis. eLife **7**, e34460.

Vlad D, Kierzkowski D, Rast MI, *et al.* 2014. Leaf shape evolution through duplication, regulatory diversification, and loss of a homeobox gene. Science **343**, 780–783.

Vuolo F, Kierzkowski D, Runions A, *et al.* 2018. LMI1 homeodomain protein regulates organ proportions by spatial modulation of endoreduplication. Genes & Development **32**, 1361–1366.

Waites R, Hudson A. 1995. *phantastica*: a gene required for dorsoventrality of leaves in *Antirrhinum majus*. Development **121**, 2143–2154.

Wuyts N, Palauqui JC, Conejero G, Verdeil JL, Granier C, Massonnet C. 2010. High-contrast three-dimensional imaging of the Arabidopsis leaf enables the analysis of cell dimensions in the epidermis and mesophyll. Plant Methods **6**, 17.